NASA-CR-168261
19840011404

NASA CR-168261
ODAI-1512-11-83

DEVELOPMENT OF A SIMPLIFIED PROCEDURE FOR ROCKET ENGINE THRUST CHAMBER LIFE PREDICTION WITH CREEP

by
M. L. Badlani
J. S. Porowski
W. J. O'Donnell
D. B. Peterson

O'DONNELL & ASSOCIATES, INC.
241 Curry Hollow Road
Pittsburgh, Pennsylvania 15236

O'DONNELL & ASSOCIATES, INC.

ENGINEERING DESIGN & ANALYSIS SERVICES

241 CURRY HOLLOW ROAD

PITTSBURGH, PENNSYLVANIA 15236

(412) 655-1200

TWX 710-667-4857

March 21, 1984

TO: DISTRIBUTION LIST FOR FINAL REPORT NASA CR 168261

Dear Sir:

Enclosed please find copies of the Final Report, "Development of a Simplified Procedure for Rocket Engine Thrust Chamber Life Prediction with Creep." The NASA number for this report is CR 168261.
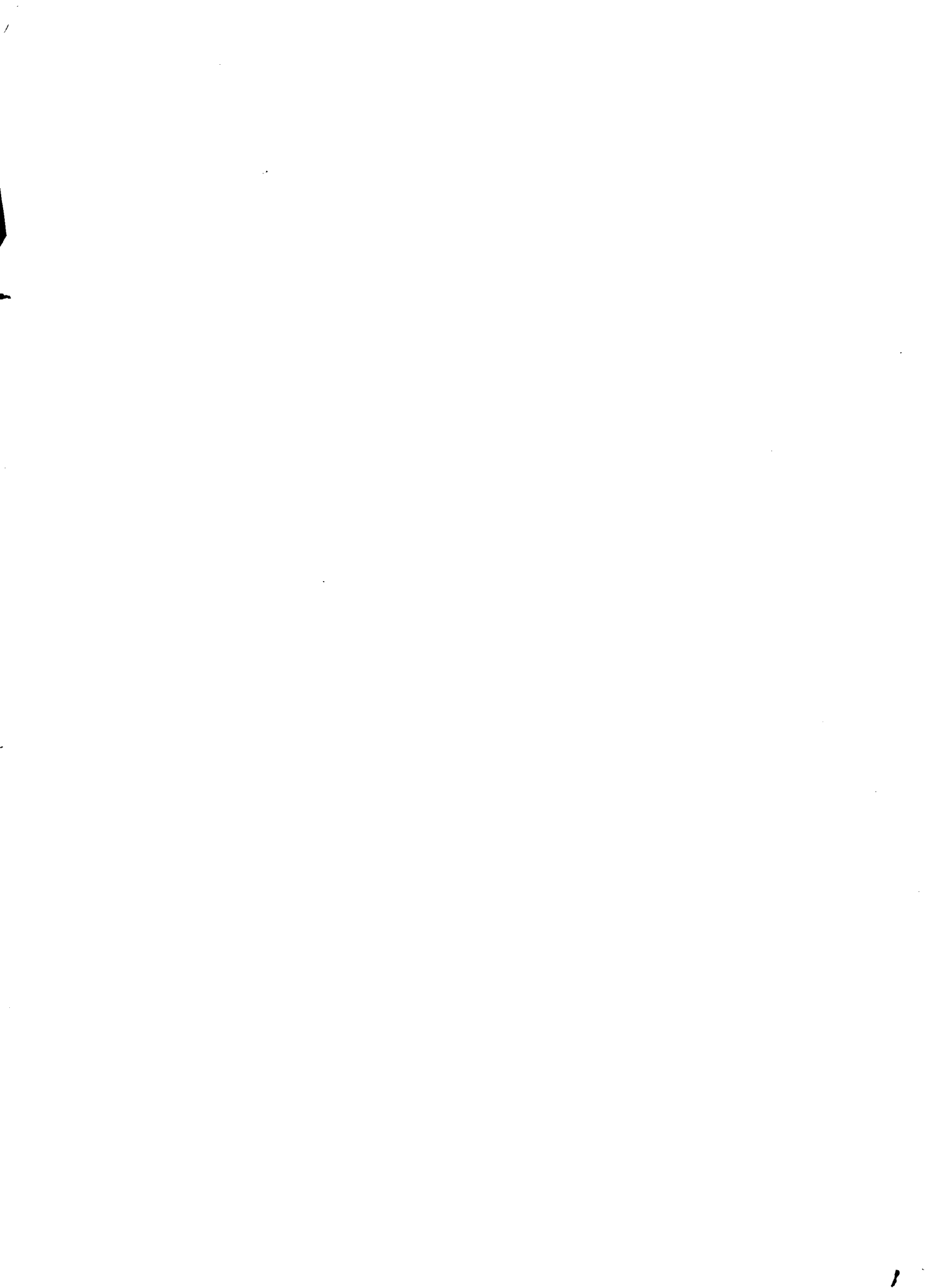
Sincerely yours,

O'DONNELL & ASSOCIATES, INC.

Janek S. Porowski
Vice President

JSP:mng

Enclosure

1. Report No.	2. Government Accession No.	3. Recipient's Catalog No. NASA CR-168261

4. Title and Subtitle	5. Report Date October 1983
Development of a Simplified Procedure for Rocket Engine Thrust Chamber Life Prediction with Creep	6. Performing Organization Code

7. Author(s)	8. Performing Organization Report No.
M. L. Badlani, J. S. Porowski, W. J. O'Donnell, D. B. Peterson	ODAI-1512-11-83
	10. Work Unit No.

9. Performing Organization Name and Address	
O'Donnell & Associates, Inc. 241 Curry Hollow Road Pittsburgh, Pennsylvania 15236	11. Contract or Grant No. NAS3-23343
	13. Type of Report and Period Covered

12. Sponsoring Agency Name and Address	Final Report
National Aeronautics & Space Administration Lewis Research Center Cleveland, Ohio 44135	14. Sponsoring Agency Code

15. Supplementary Notes

H. J. Kasper, NASA Technical Monitor

16. Abstract

An analytical method for predicting engine thrust chamber life is developed. The method accounts for high pressure differentials and time-dependent creep effects both of which are significant in limiting the useful life of the shuttle main engine thrust chamber. The hot-gas-wall ligaments connecting adjacent cooling channel ribs and separating the coolant flow from the combustion gas are subjected to a high pressure induced primary stress superimposed on an alternating cyclic thermal strain field. The pressure load combined with strain-controlled cycling produces creep ratcheting and consequent bulging and thinning of these ligaments. This mechanism of creep-enhanced ratcheting is analyzed for determining the hot-gas-wall deformation and accumulated strain. Results are confirmed by inelastic finite element analysis. Fatigue and creep rupture damage as well as plastic tensile instability are evaluated as potential failure modes. It is demonstrated for the NARloy Z cases analyzed that when pressure differentials across the ligament are high, creep rupture damage is often the primary failure mode for the cycle times considered.

17. Key Words (Suggested by Author(s))	18. Distribution Statement
Rocket Engines, nozzles, thrust chambers, structural fatigue, creep rupture, plastic tensile instability, stress analysis.	Unclassified - Limited

19. Security Classif. (of this report)	20. Security Classif. (of this page)	21. No. of Pages	22. Price*
Unclassified	Unclassified	90	

N84-19472 #

NASA C-168 (Rev. 10-75)

DEVELOPMENT OF A SIMPLIFIED PROCEDURE FOR ROCKET ENGINE
THRUST CHAMBER LIFE PREDICTION WITH CREEP

TABLE OF CONTENTS

DEVELOPMENT OF A SIMPLIFIED PROCEDURE FOR ROCKET ENGINE THRUST CHAMBER LIFE PREDICTION WITH CREEP

SUMMARY

An analytical method for predicting engine thrust chamber life is developed. The method accounts for high pressure differentials and time-dependent creep effects both of which are significant in limiting the useful life of the shuttle main engine thrust chamber. The hot-gas-wall ligaments connecting adjacent cooling channel ribs and separating the coolant flow from the combustion gas are subjected to a high pressure induced primary stress superimposed on an alternating cyclic thermal strain field. The pressure load combined with strain-controlled cycling produces creep ratcheting and consequent bulging and thinning of these ligaments. This mechanism of creep-enhanced ratcheting is analyzed for determining the hot-gas-wall deformation and accumulated strain. Results are confirmed by inelastic finite element analysis. Fatigue and creep rupture damage as well as plastic tensile instability are evaluated as potential failure modes. It is demonstrated for the NARloy Z cases analyzed that when pressure differentials across the ligament are high, creep rupture damage is often the primary failure mode for the cycle times considered.

DEVELOPMENT OF A SIMPLIFIED PROCEDURE FOR ROCKET ENGINE
THRUST CHAMBER LIFE PREDICTION WITH CREEP

1.0 INTRODUCTION

Life predictions of regeneratively liquid-cooled rocket engine thrust chambers have usually been based on low cycle fatigue evaluations. Experiments, however, have shown that low-cycle fatigue is not always the controlling failure mode. The chamber coolant walls progressively thin and bulge with each firing cycle until failure occurs due to tensile instability. In a recent report for NASA [1],* an analysis of the deformation and strain accumulation due to plastic ratcheting of the hot-gas-wall due to successive firings of a cylindrical test chamber was performed. The tensile instability mode of failure was analyzed as well as low-cycle fatigue. A simplfied analytical procedure for predicting thrust chamber life was developed.

The analyses of [1], however, were for an experimental cylindrical thrust chamber where the pressure differential between the coolant channel and the combustion gas chamber is significantly lower than the corresponding pressure differential in the space shuttle main engine (SSME). In addition, the experimental engine firing period is limited to several seconds, whereas the SSME engine firing time is measured in minutes.

The procedure developed in [1], therefore, does not include any creep and is applicable only for short cycle times. For the SSME thrust chamber where cycle times are much longer, the time-dependent response of the material must be included in the creep ratcheting analysis. The higher pressure differential in the SSME thrust chamber must also be considered. The present work is aimed at developing a simplified method for predicting the number of times the SSME can be fired before the liner ligaments fail. The method would allow the designer to optimize the various engine design parameters to achieve longer life. The accuracy of the simplified method

---

*Numbers in brackets refer to References at end of Report.

is verified via the finite element technique by performing one or two cycles of inelastic analysis on a simple ligament beam model.

The scope of the work is as follows:

1. - Development of the creep-ratcheting solution for determination of ligament (hot-gas-wall) deformation and strain accumulation.

2. - Analysis of failure modes and criteria. Develop failure criteria by investigating:

(a) fatigue

(b) creep rupture damage, and

(c) plastic/creep tensile instability

3. - Synthesize a simple design procedure for predicting thrust chamber life based on 1 and 2 above and provide sample calculations.

Each of these items will be discussed in the sections to follow. The assumptions made in the development of the analysis procedure for each item are discussed in their respective sections.

2.0 DEVELOPMENT OF THE CREEP RATCHETING SOLUTIONS FOR DETERMINATION OF HOT-GAS-WALL DEFORMATION AND STRAIN ACCUMULATION

2.1 Description of the thrust chamber

The experimental plug nozzle thrust chamber is shown in Figure 1. This figure shows a typical plug nozzle assembly consisting of the contoured centerbody and flanged cylinder along with the cross-sectional details of the cylinder. The inner liner of the cylinder contains axial flow coolant channels similar to those of the SSME thrust chamber. The inner wall separating the coolant flow and the combustion gas is subjected to severe thermal cycling during startup and shutdown.

Thrust Chamber Assembly

Contoured
Centerbody

Cylinder

Injector End

Cylinder Flange
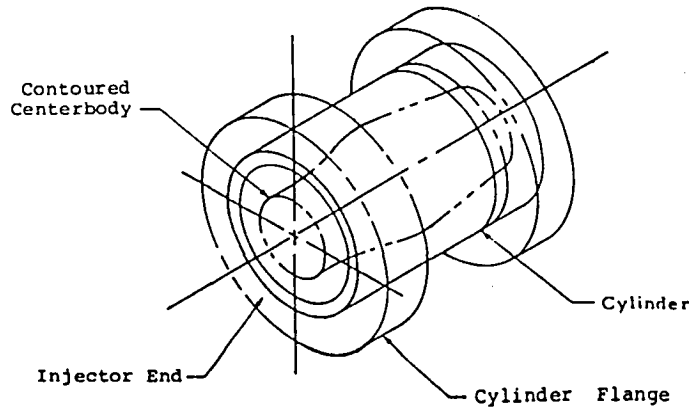
Cylinder Cross Section

Closeout Wall

Combustion Gas
Side

CLOSE-OUT WALL

Coolant
Channel

P

Rib

Ligament

2H

Inner Wall

σ_b
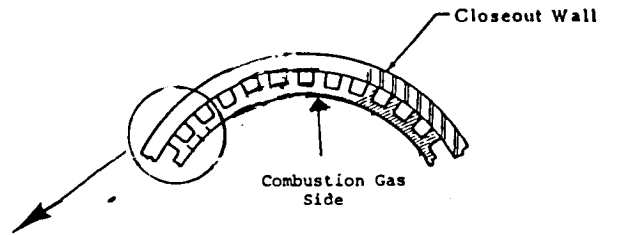
FIGURE 1   PLUG NOZZLE THRUST CHAMBER

4

The ligaments in the SSME thrust chamber are subjected to higher differential pressure between the coolant channels and the combustion gas side of the liner and longer firing cycles than the experimental chamber. The high primary stress due to this differential pressure is superimposed on the alterlating cyclic thermal straining. The pressure load combined with strain-controlled cycling produces creep ratcheting and consequent bulging and thinning of the ligaments. This mechanism of creep-enhanced ratcheting is analyzed to develop an analytical model for determining the hot-gas-wall deformation and accumulated strain.

2.2 Inelastic Strains

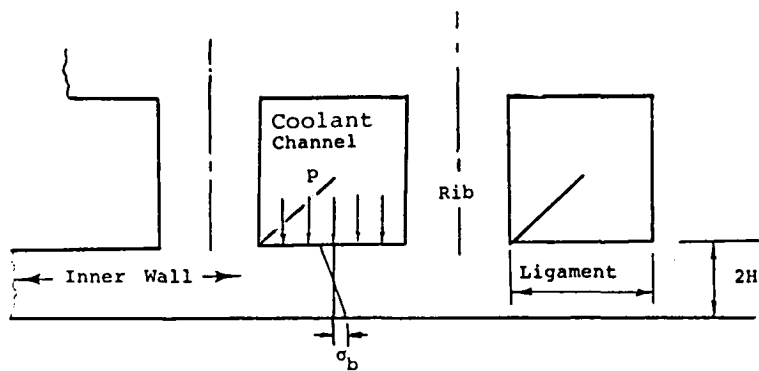The hystersis loop for a typical loading cycle, not including the initial chilldown, is shown schematically in Figure 2. OA and AB represent the initial elastic and plastic portions during heat up. Creep occurs during operation at elevated temperature causing the stresses to redistribute. The stress field generated after severe plastic straining is compressive at the peak of the transient and tends to relax asymptomatically to the stationary state related to the sustained primary load due to pressure. The relaxation of the thermally induced stresses due to creep results in the creep-enhanced ratcheting mechanism mentioned above. The creep relaxation is depicted by the vertical line BC in the figure. CD and DE represent the elastic and plastic portions during cool down. Due to creep relaxation, initial yielding occurs earlier resulting in a larger plastic portion. Thus, as a result of including creep, the elastic portion is reduced and the plastic portion increased.

Denoting the average temperatures of the ligament and closeout wall by T_i and T_o, respectively. The inelastic strain range in the hoop direction due to differential thermal expansion EB and creep relaxation BC, is given by:

$$\Delta\varepsilon'_{p_1} = \left[\left(T_i\alpha_i - T_o\alpha_o\right)_{max} - \left(T_i\alpha_i - T_o\alpha_o\right)_{min}\right] - \left(S_{y_{max}} + S_{y_{min}}\right)/E + \Delta\sigma_c/E \quad (1)$$
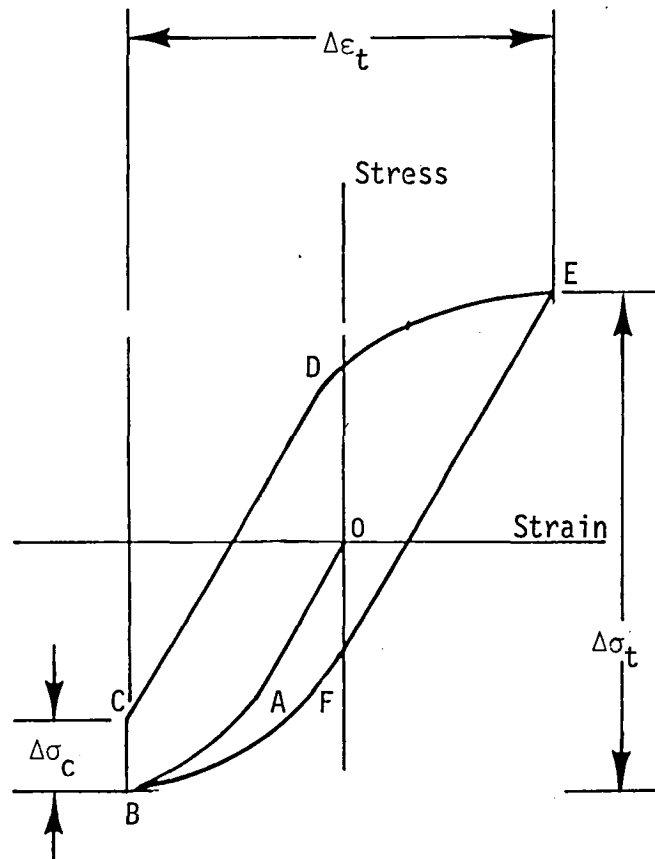
FIGURE 2   TYPICAL LOADING CYCLE LOOP

where α_i and α_o are the thermal expansion coefficients of the ligament and closeout, respectively, and $(T_i\alpha_i - T_o\alpha_o)_{max}$ and $(T_i\alpha_i - T_o\alpha_o)_{min}$ are the maximum and minimum thermal strains, respectively, that occur during the loading cycle. $\Delta\sigma_c$ is the relaxation stress and $S_{y_{max}}$ and $S_{y_{min}}$ are respectively the ligament material absolute yield strengths corresponding to the ligament average temperatures at the time in the cycle when $(T_i\alpha_i - T_o\alpha_o)_{max}$ and $(T_i\alpha_i - T_o\alpha_o)_{min}$ are calculated. The inelastic compressive strain generated within the EBC part of the cycle is reversed by plastic straining along the CDE line.

Though $\Delta\varepsilon'_{p_1}$ as given by Equation (1) accounts for the major portion of the inelastic strain range in the hoop direction, there is also a temperature drop across the ligament which causes bending, since the ligament ends are constrained. This thermally induced bending, though acting only for a short portion of the cycle, may enhance the ratchet strain. Its effect may be assessed by computing the elastic energy of the thermally induced bending stresses and correcting the hoop strain accordingly. Conservatively assuming that all of the available elastic energy goes into plastic straining of the ligament, the correction due to thermally induced bending is given by [1]:

$$\Delta\varepsilon''_{p_1} = \frac{E(\alpha\Delta T)^2}{12(1-\nu)^2 S_y} \tag{2}$$

where ΔT is the temperature drop across the ligament.

The total inelastic strain in the hoop direction for the complete cycle is thus:

$$\varepsilon_1 = 2\left(\Delta\varepsilon'_{p_1} + \Delta\varepsilon''_{p_1}\right) \tag{3}$$

2.3 Creep relaxation

For low pressures, as in the case of the experimental thrust chambers, the relaxation of stress can be determined by using the uniaxial solution for zero total strain rate. Assuming Norton's law governs creep flow:

$$\dot{\varepsilon} = B\sigma^r \qquad (4)$$

where B and r are material constants, the governing differential equation is:

$$\frac{1}{E}\frac{d\sigma}{dt} + B\sigma^r = 0 \qquad (5)$$

On integrating, the stress after relaxation within time t is given by

$$\sigma = \sigma_p[1 + \tau(r-1)]^{1/1-r} \qquad (6)$$

where σ_p = peak stress, and

$\tau = BE\sigma_p^{r-1} t$ denotes nondimensional time

Here, $\sigma_p = S_y$, the yield stress. Thus the creep relaxation stress is given by:

$$\Delta\sigma_c = (S_y - \sigma) \qquad (7)$$

Equation (6) has been verified by finite element analysis and found to be very accurate for predicting the mid-plane relaxation stresses for the low pressure cases. When the pressures are high, however, the relaxation proceeds faster and reaches the steady state much more rapidly. Figure 3 shows the mid-plane stress relaxation curves for the case of no pressure (which is coincident with the finite element results for the low pressure case of 547 psi) as given by Equation (6) and the case of high pressure

8

$$\dot{\epsilon} = B\sigma^r$$
$$B = 5.5225 \times 10^{-7}$$
$$r = 6.65$$
$$\sigma - ksi$$
$$E = 16.35 \times 10^6 \text{ psi } (112729 \text{ MPa})$$

p = 0 (Analytical, Equation 6)
p = 3000 psi (20.68 Mpa)

STRESS, KSI (MPa)

-30 (-206.84)
-20 (-137.9)
-10 (-68.95)
0

40   80   120   160   200   240   280

TIME, SECONDS
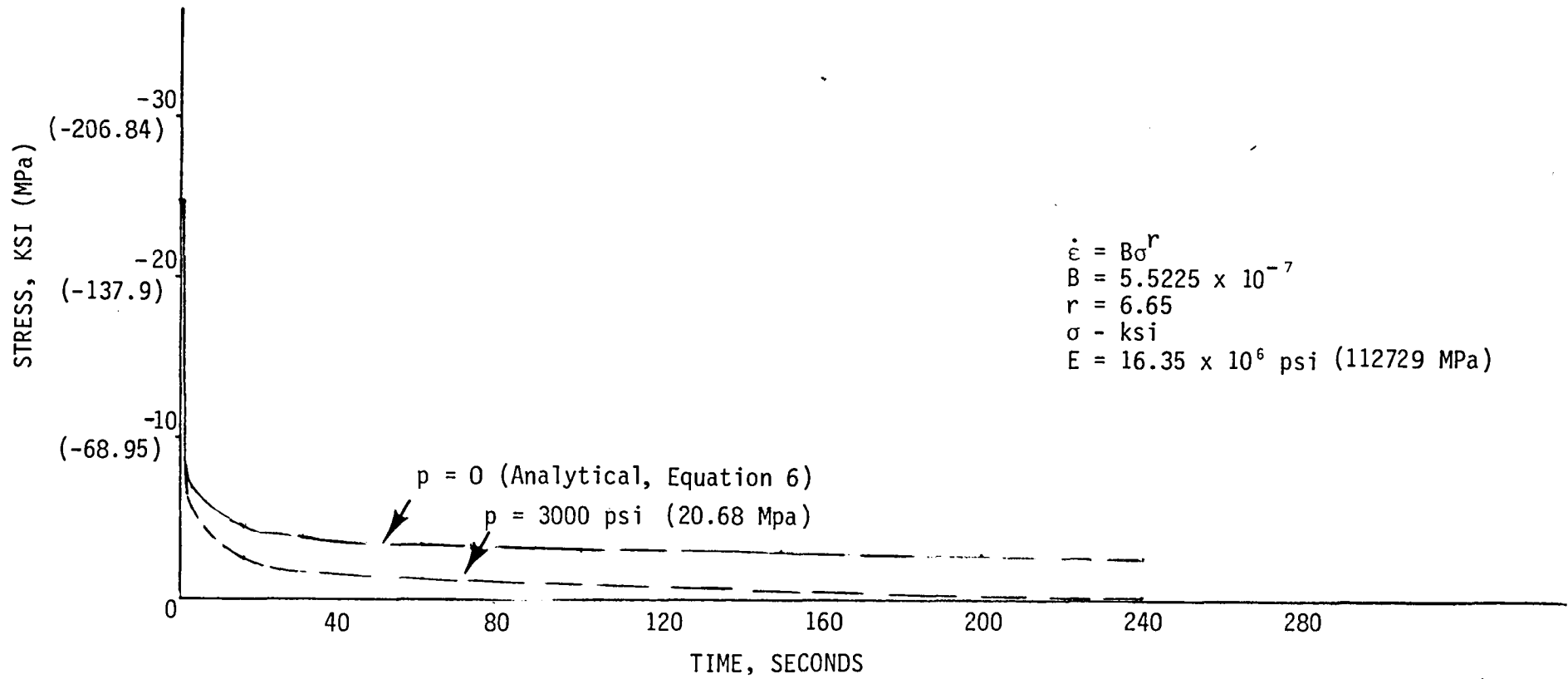
FIGURE 3a STRESS RELAXATION CURVES (MID-SURFACE)

(p = 3000 psi) as obtained from finite element analysis described later
in the report. It is seen that for the high pressure case the mid-plane
stress relaxes to almost zero and hence the creep relaxation stress is
given by :

$$\Delta\sigma_c = S_y \qquad\qquad (8)$$

For intermediate pressure cases, the relaxation stress may be obtained
by interpolation from Figure 3. For conservative evaluation, Equation
(8) may be conveniently used in all pressure cases.

The relaxation curves plotted in Figure 3a have been obtained by using
the creep law constants for NarloyZ at 1325°F. Stress relaxation curves
that are applicable in the general case can be generated from Equation (6)
for the zero pressure condition by plotting the dimensionless stress para-
meter σ/σ_p vs. nondimensional time τ for various r. These curves are
shown in Figure 3b and may be used for estimating $\Delta\sigma_c$ when the pressure
differentials are lower than 1000 psi. For higher pressure differentials,
Eq. (8) is applicable in the general case.
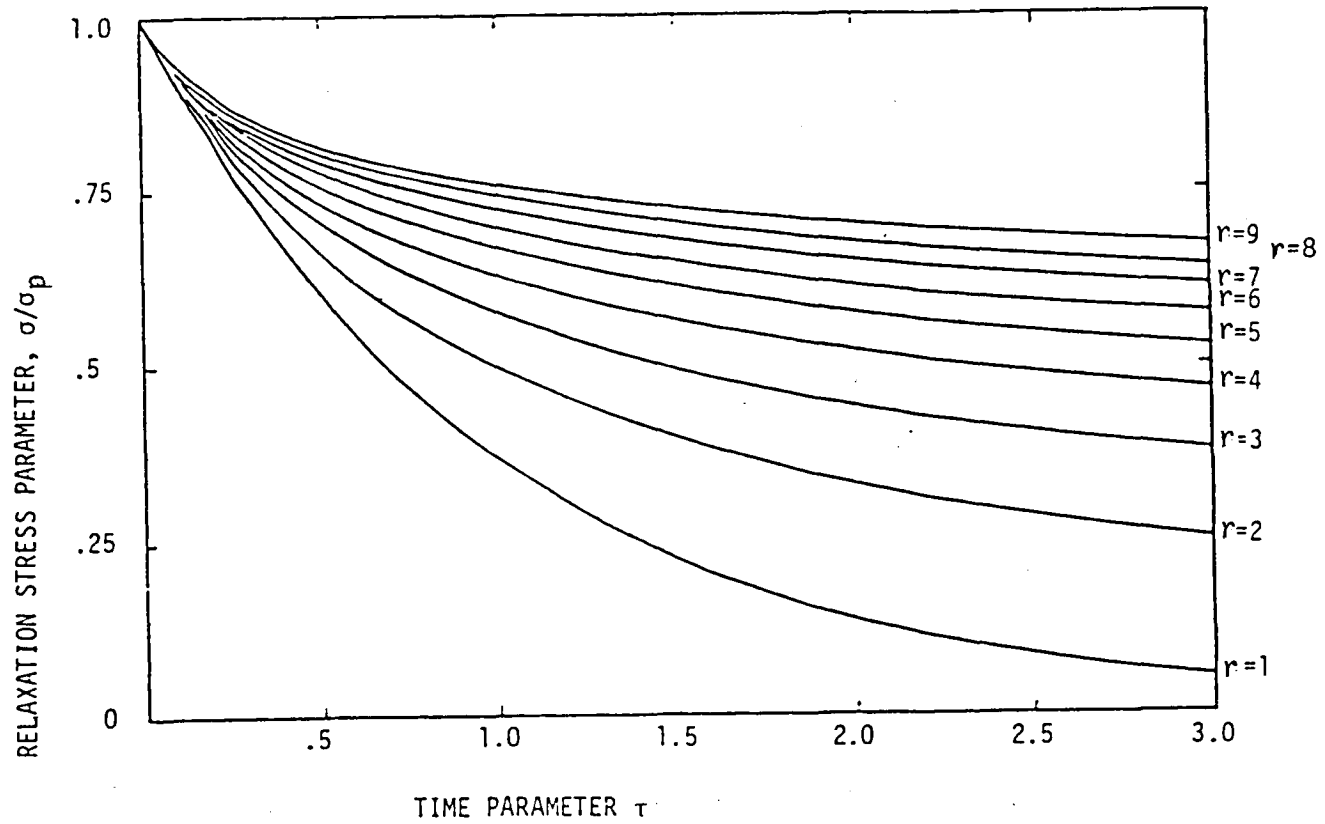
FIGURE 3b STRESS RELAXATION CURVES FOR NORTON CREEP LAW

11

2.4 Incremental deformation of ligament

The corresponding curvature and hence the deflection is determined using the method developed in [1]. The method uses a yield surface for combined bending and membrane loading to determine the incremental inward bulging and progressive thinning near the center of the ligaments at the inner liner of the thrust chamber. The derivation details are given in [1] and hence only an outline is presented here.

2.4.1 Mechanics of inelastic distortion

The approach used to determine the strain increments within the load cycles is explained in Figure 4. The beam of Figure 4a simulates the response of the ligament subjected to pressure-induced bending and cyclic straining in the hoop direction. The yield surface for a beam subjected to bending and hoop force is given by [2]:

$$m + n^2 - 1 = 0 \qquad\qquad (9)$$

where m and n are dimensionless variables defined by:

$$m = \frac{M}{M_o} \qquad\qquad (10a)$$

$$n = \frac{N}{N_o} \qquad\qquad (10b)$$

In the above, N and M denote the hoop force and bending moment, while N_o and M_o denote the yield hoop force and yield bending moment given by:

$$N_o = 2H\, S_y \qquad\qquad (11a)$$

$$M_o = H^2\, S_y \qquad\qquad (11b)$$

for a rectangular beam of unit width, height 2H and yield stress S_y.

If shear is also included in the model, the yield surface is three-dimensional as shown in Figure 5 and is given by [3]:

12

a)
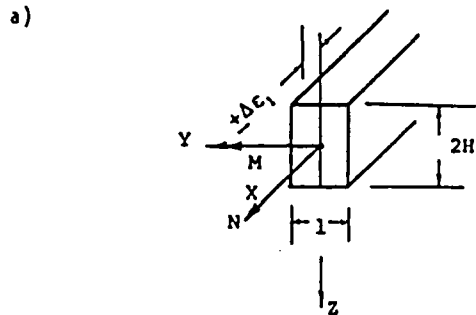
X – Hoop Direction
Y – Axial Direction
Z – Radial Direction

b)

Plastic Contrac-
tion of Liga-
ment

loading pass

Plastic Contraction of Ligament

$n^2 + m - 1 = 0$

Bending Component θ

Plastic Stretching
of Ligament

Known hoop
component λ
of resulting
plastic strain
vector

$n = N/N_o = N/(2H\ S_y)$
$m = M/M_o = M/(H^2\ S_y)$
$\lambda = 2\ H\dot{\epsilon}$
$\dot{\theta} = H^2\dot{K}$
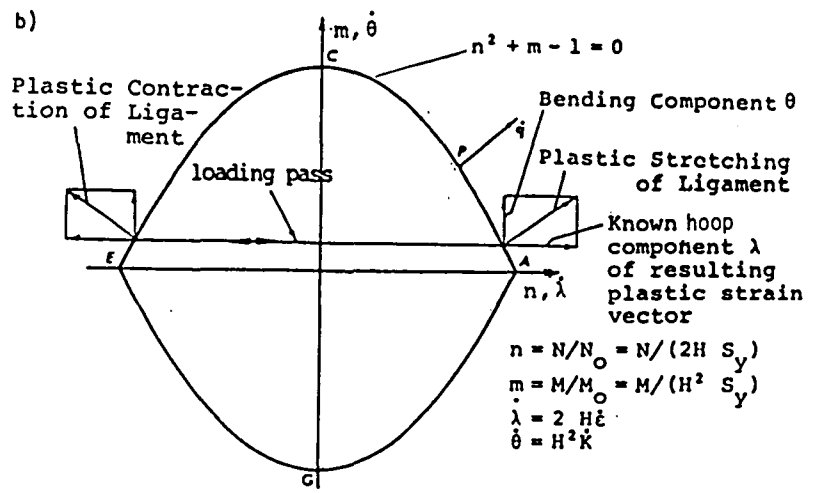
FIGURE 4   PLASTIC RATCHET IN A BAR OF RECTANGULAR
CROSS SECTION SUBJECTED TO SUSTAINED
BENDING MOMENT AND CYCLIC HOOP STRAIN

13

Yield Surface:
$$m\sqrt{1-s^2} + n^2 + s^2 = 1$$
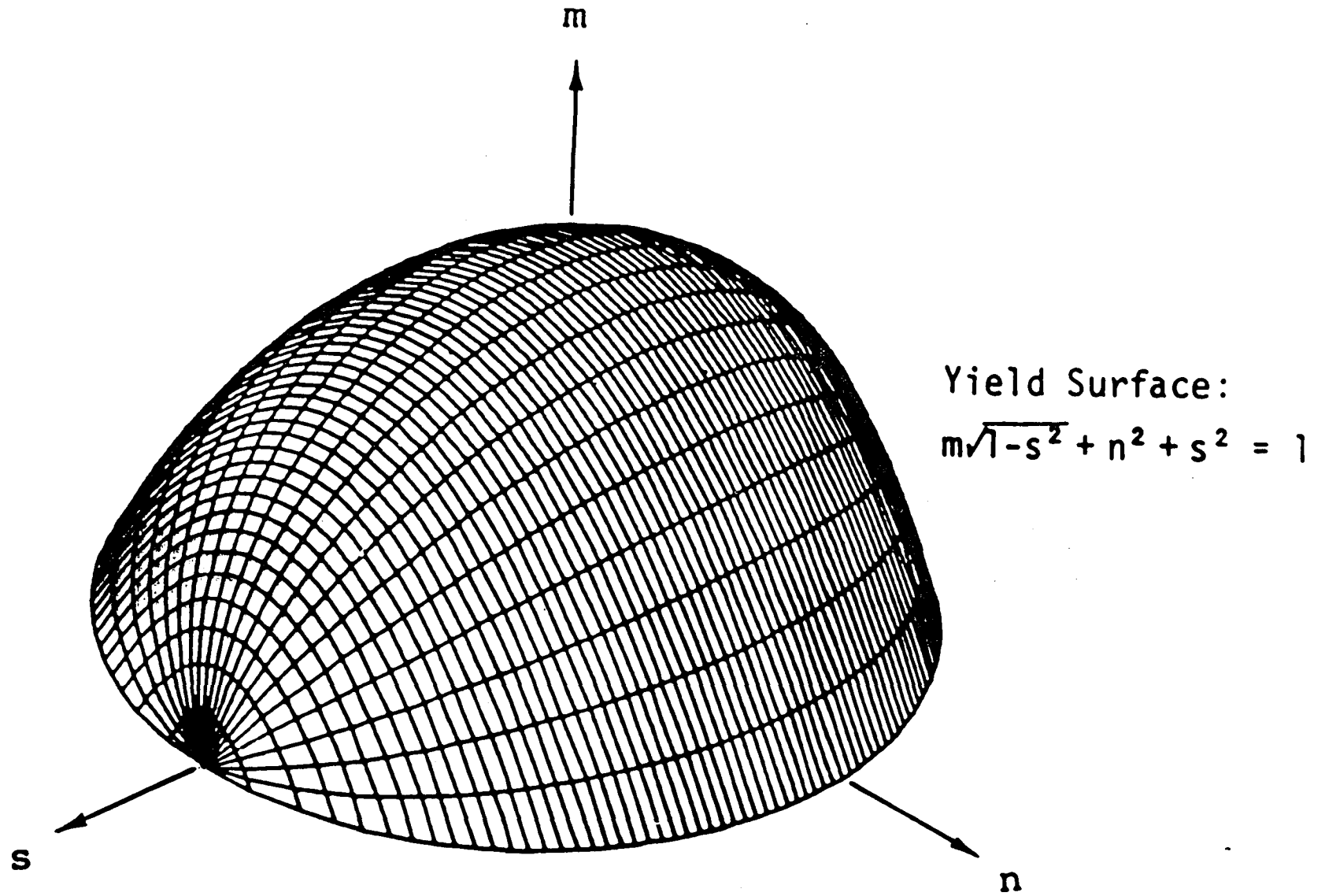
FIGURE 5   YIELD SURFACE FOR COMBINED BENDING, SHEAR AND MEMBRANE LOADING

$$m + \frac{n^2}{k} - k = 0 \qquad (12)$$

where

$$k = \sqrt{1 - s^2} \qquad (13)$$

and $s = \frac{2\tau}{S_y}$ is the dimensionless shear stress.

Using the normality law, the generalized strain rates are:

$$\dot{\lambda} = \bar{A} \frac{\partial F}{\partial n} = 2\bar{A}n \qquad (14a)$$

$$\dot{\theta} = \bar{A} \frac{\partial F}{\partial m} = \bar{A} \sqrt{1 - s^2} \qquad (14b)$$

$$\dot{\phi} = \bar{A} \frac{\partial F}{\partial s} = \bar{A} \left(2s - \frac{ms}{\sqrt{1 - s^2}} \right) \qquad (14c)$$

where $\bar{A}$ is an arbitrary positive scalar and $\dot{\lambda}$, $\dot{\theta}$, $\dot{\phi}$ are the generalized hoop, curvature and shear strain rates respectively. The relationship between the generalized strain rates and the hoop strain rate, curvature rate and shear strain rate are, respectively [1]:

$$\dot{\lambda} = 2H\dot{\varepsilon}_1 \qquad (15a)$$

$$\dot{\theta} = H^2 \dot{K} \qquad (15b)$$

$$\dot{\phi} = H\dot{\gamma} \qquad (15c)$$

From Equations (3), (14) and (15), the curvature and shear strain are, respectively:

$$K = \frac{\sqrt{1-s^2}}{n} \frac{\varepsilon_1}{H} \tag{16}$$

and

$$\gamma = \left(2s - \frac{ms}{\sqrt{1-s^2}}\right)\left(\frac{\varepsilon_1}{n}\right) \tag{17}$$

The curvature and shear strain as determined from Equation (16) and (17) for each cross-section can then be integrated along the length of the ligament to obtain the corresponding bending deflection δ_1 and shear deflection δ_2.

2.4.2 Creep-induced deflection

In addition to δ_1 and δ_2, the steady creep strain due to pressure also contributes to the total deflection. This additional deflection is determined by treating the ligament as a clamped beam under uniform loading, as described below.

Consider the beam of rectangular cross-section shown in Figure 6. Then Bernoullis' approximation of plane sections gives for the strain rate at point P in the x-direction:

$$\dot{\varepsilon}_x = -z \frac{\partial^3 v}{\partial x^2 \partial t} = -z\dot{v}'' \tag{18}$$

Using Norton's Creep Law:

$$\dot{\varepsilon}_x = B\sigma_x^r \tag{19}$$

where B and r are material constants, gives:

$$\sigma_x = \frac{1}{B^{1/r}} (\dot{v}'')^{1/r} z^{1/r} \tag{20}$$

The bending moment M is given by:

$$M = \int_A z\sigma_x dA \tag{21}$$

16
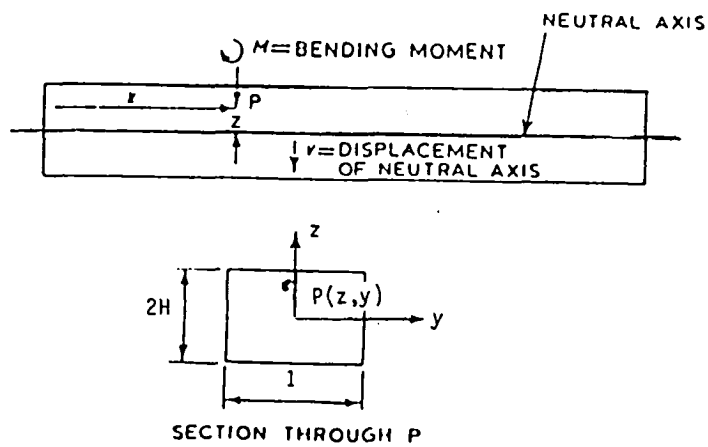
FIGURE 6   CO-ORDINATE SYSTEM AND BEAM DIMENSIONS
FOR DERIVATION OF EQUATION (22)

where A is the cross-sectional area of the beam. Substituting from (20), the following differential equation is obtained for the deflection of the beam:

$$v'' = -Bt \left(1 + \frac{1}{2r}\right)^r \left(\frac{1}{H^2}\right)^r \frac{1}{H} M^r \tag{22}$$

Following [4], for the ligament under pressure loading, Figure 7:

$$M = - \frac{p\bar{m}^2}{2} \left[1 - \left(\frac{\ell/2 - x}{\bar{m}}\right)^2\right] \tag{23}$$

where $\bar{m}$ is a constant to be determined from the boundary conditions. Using (23) and the clamped boundary conditions i.e., $v' = 0$ at $x = 0$, ℓ, gives the maximum deflection:

$$v_{max}(r) = \delta_3 = - \frac{Bt\ell^2}{4H} \left(\frac{p\ell^2}{16H^2}\right)^r \bar{F}(r) \tag{24}$$

where $\bar{F}(r)$ has been tabulated for various r in Table I. For details of the derivation of (24), the reader is referred to [4].

Thus total deflection per cycle

$$\delta = \delta_1 + \delta_2 + \delta_3 \tag{25}$$

2.4.3 Ligament distortion

Experimental evidence shows that the deformed shape of the ligament can be approximated by a linear variation in thickness as shown in Figure 8. Thus using the linear thinning model developed in [1], the thinning after N cycles is then given by:

$$t_N = \frac{N \delta w}{(\ell + w)} \tag{26}$$

where ℓ is the width of the ligament in the hoop direction and w is the width of the rib.

18
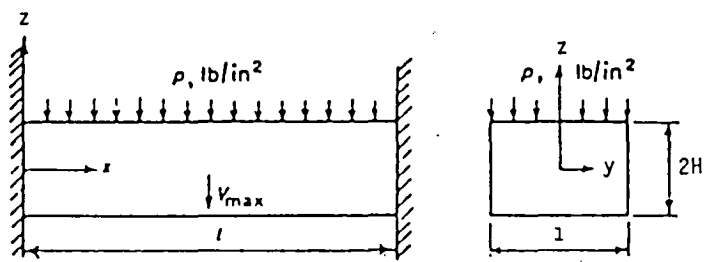
Uniformly loaded, clamped beam co-ordinate system.

FIGURE 7   LIGAMENT UNDER PRESSURE LOADING

TABLE I

r	1	2	3	4	5
$\overline{F}(r)$	0·250	0·206	0·170	0·148	0·133

r	6	7	8	9	10
$\overline{F}(r)$	0·122	0·114	0·105	0·100	0·093

Values of $\overline{F}(r)$ in Equation (24) for maximum
deflection of clamped beam.
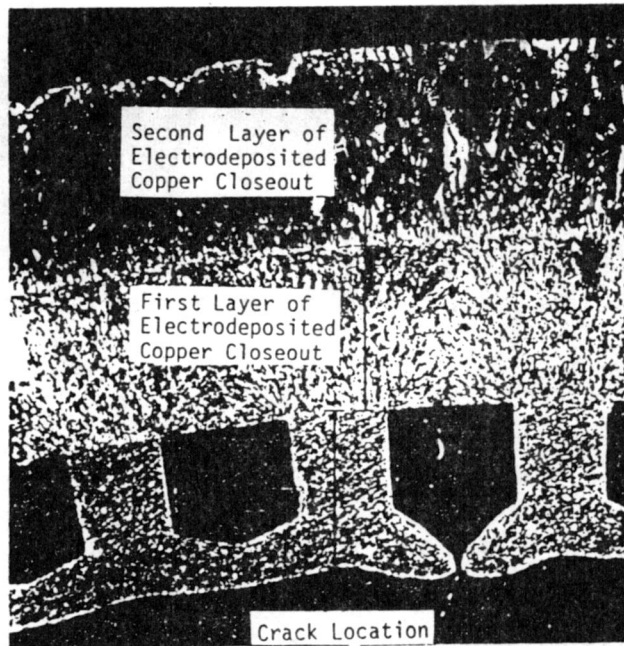
FIGURE 8a TYPICAL COOLING CHANNEL WALL FAILURE

$$t(x) = (t_{max} - t_{min})\frac{2x}{\ell} + t_{min}$$
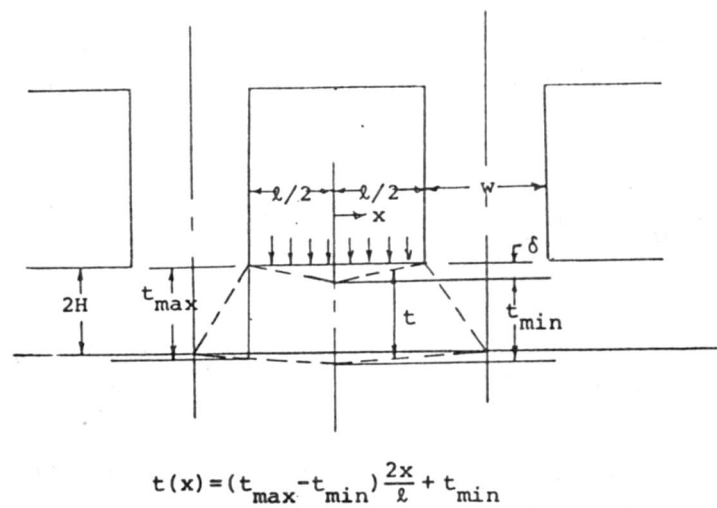
FIGURE 8b LIGAMENT LINEAR THINNING MODEL

3.0 ANALYSIS OF FAILURE MODES AND CRITERIA

The ligaments are subjected to incremental permanent deformations during each firing cycle of the thrust chamber. The geometry of these ligaments changes as the incremental strains accumulate. They are subjected to incremental bulging and progressive thinning near the center of the ligament. Fatigue and creep rupture damage as well as plastic tensile instability are considered as potential failure modes and evaluated herein.

3.1 Fatigue

The strain range at the minimum ligament section increases with progressing distortion and thinning. For fatigue calculations, the maximum local hoop strain range at the minimum ligament section can be obtained from the average hoop strain range by integration if the geometry of the distorted ligament is known. The method of determining the maximum local strain range in the minimum ligament section is the same as that developed in [1] and hence not repeated here. For the linear thinning model of Figure 8b, the effective strain range in the minimum ligament section for entering the fatigue curve is then:

$$\overline{\varepsilon}_{min} = \frac{2}{\sqrt{3}} \sqrt{\varepsilon_{1}^{2}{}_{min} + \varepsilon_{1min}\varepsilon_{2min} + \varepsilon_{2}^{2}{}_{min}} \tag{27}$$

where ε_{1min}, the local hoop strain in the minimum ligament section is:

$$\varepsilon_{1min} = \varepsilon_{1avg} \frac{q-1}{q} \left(\frac{t_{max}}{t_{min}} - 1\right) \left[\left(\frac{t_{max}}{t_{min}}\right)^{\frac{q-1}{q}} - 1\right]^{-1} \tag{28}$$

and q is the exponent in the Ramberg-Osgood type stress strain relation $\varepsilon = A\sigma^{q}$. The average hoop strain is given by:

$$\varepsilon_{1avg} = \alpha(T_{i} - T_{o}) \tag{29a}$$

The axial strain ε_{2min} in the minimum ligament section is also given by:

22

$$\varepsilon_{2min} = \alpha(T_i - T_o) \tag{29b}$$

where T_i is the average temperature of ligament and T_o is the average temperature of closeout.

For the linear variation assumed, the thickness t_{min} and t_{max} after the Nth cycle are given by:

$$t_{min} = \frac{2H(\ell + w) - N \delta w}{(\ell + w)} \tag{30}$$

$$t_{max} = \frac{2H(\ell + w)^2 + N \delta \ell w}{(\ell + w)^2} \tag{31}$$

where δ is the deformation per cycle from (25).

Equations (27) through (31) along with the fatigue curve are then used to determine the fatigue life. Note that though the procedure parallels that in [1], the resulting strain range is not the same, since the deflection and hence the thinning per cycle is now larger due to creep effects.

3.2 Creep Rupture Damage

The compressive stress field generated at the peak of the transient relaxes during the creep period to the steady state pressure stress. When the pressure acting on the ligament is low, as in the case of the experimental thrust chamber, the finite element results show that there is negligible redistribution of the bending stress due to pressure and the hoop stress generated by the thermal transient remains compressive up to the end of the creep period. Thus, creep rupture damage is not a potential failure mode for such cases.

When the pressure acting on the ligament is higher, as in the SSME thrust chamber, the finite element results show that the hoop stress relaxes quite rapidly becoming tensile on the hot-gas-wall surface of the ligament. The pressure stress is redistributed during the creep period and relaxation occurs to this steady state value. Thus creep rupture damage must be included in the failure analysis for high pressure cases.

The stress relaxation curves for the hot-gas-wall surface of the ligament are shown in Figure 9 for the two pressure cases discussed. Interpolation between these curves may be used to obtain the relaxation curves for intermediate pressure cases. Also, the curves can provide an estimate of the time over which the stress remains tensile for consideration in the creep rupture damage analysis.

The creep rupture damage evaluation is based on the tensile stress at the end of the creep period. This may or may not be the steady state stress. Since the creep period is known, the time for the pressure stress to redistribute must be less than this creep period for it to reach its steady state value. This time may be estimated by using Calladine's work, [5]. He has derived a simple formula for the time taken for the redistribution of stress in a structure from an initial state to a final steady state to be practically complete. The time taken is expressed in terms of the time taken for creep strain to become equal to a certain multiple of the elastic strain in a constant stress creep test performed at a stress level which depends on the steady state stress in the structure. This time for redistribution is given by:

$$t_{ss} = \frac{1}{B\sigma_{ss}^r} \frac{2.3}{r} e \tag{32}$$

where

σ_{ss} = steady state stress
e = elastic strain
B and r are constants in the creep law.

Though the above formula was derived for kinematically determinate structures, it provides a reasonable estimate for the redistribution of mid-channel pressure stress in the present case.

The finite element results for the clamped beam model show that for the creep exponent $r = 6.65$, the mid-channel steady state stress at the

24

$$\dot{\varepsilon} = B\sigma^r$$
$$B = 5.5225 \times 10^{-7}$$
$$r = 6.65$$
$$\sigma - ksi$$
$$E = 16.35 \times 10^6 \text{ psi} \quad (112729 \text{ MPa})$$

p = 547 psi (3.77 MPa)

p = 3000 psi (20.68 MPa)
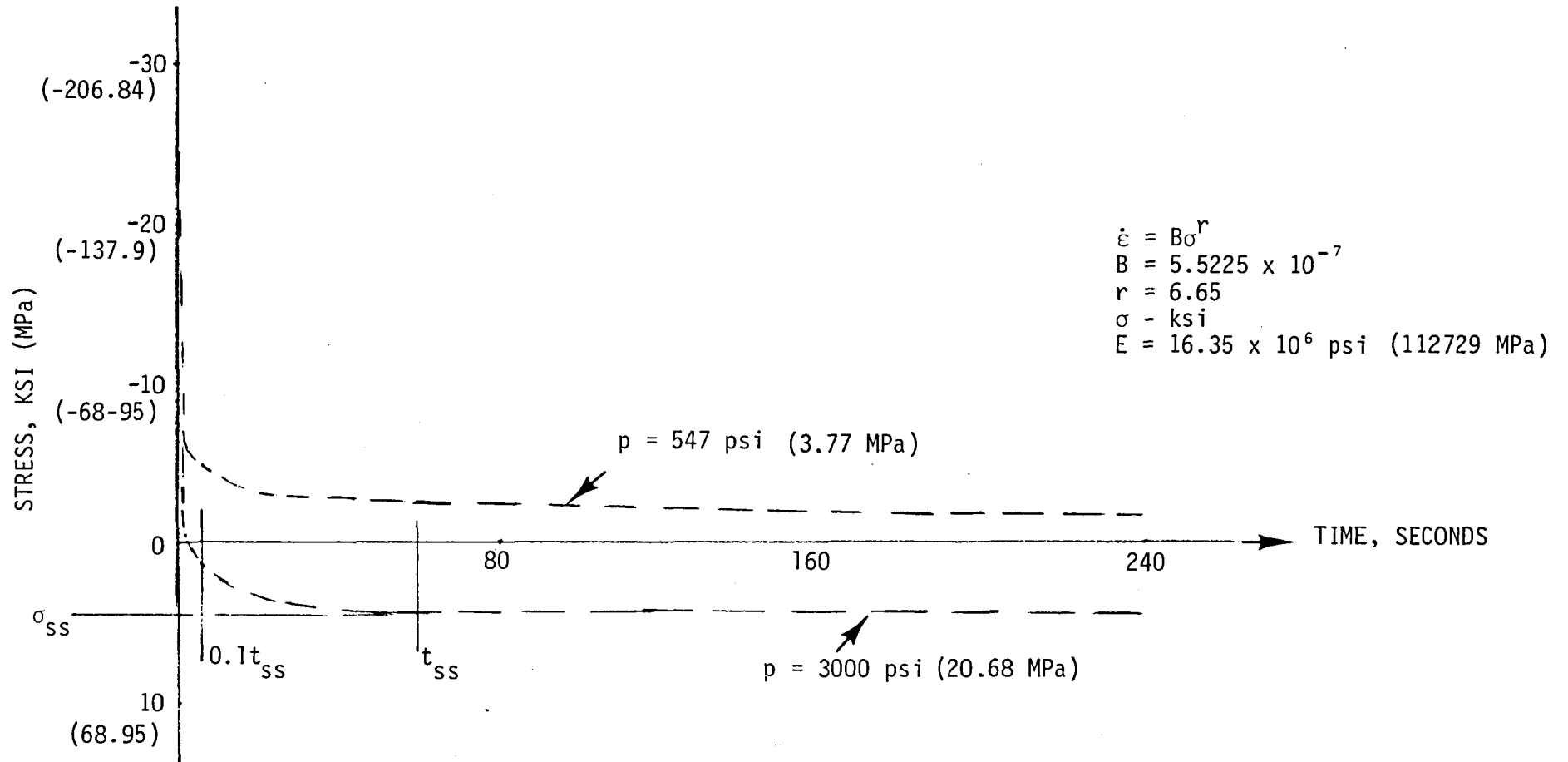
FIGURE 9   STRESS RELAXATION CURVES (HOT-GAS-WALL SURFACE)
FOR NARLOY Z FROM FINITE ELEMENT ANALYSIS

surface is approximately 0.8 of the initial bending stress. Calladine in [6] has studied several structures subject to creep for determining the way in which the greatest stress in the structure varies with the creep exponent r when the geometry and the loading remain unchanged. He showed that a linear interpolation between the cases r = 1 (elastic) and r = ∞ (perfectly plastic) may be used for estimating the greatest steady state stress for arbitrary r. Following this thought, the steady state stress in the present case may then be estimated by:

$$\sigma_{ss} = F\sigma_{in} \tag{33}$$

where σ_{in} is the initial stress and F is plotted for various r in Figure 10. This plot has been generated by connecting the two known values of F at r = 1 and r = 6.65. The maximum initial elastic stress can be determined using, for example, finite element solution. Its value can also be estimated with sufficient accuracy by treating the ligament as a clamped beam under pressure loading.

Having determined the steady state stress from (33), this is substituted in (32) to estimate redistribution time t_{ss}. If t_{ss} is less than the cycle creep period, creep rupture damage evaluation is based on σ_{ss}. If, however, t_{ss} is greater than the cycle creep period, creep rupture damage is usually small and may often be excluded from failure evaluation. Since the stress on the hot-gas-wall surface must become tensile before reaching the steady state value, a case could conceivably arise where the stress has become tensile but did not quite reach σ_{ss} by the end of the creep period. In order to provide conservative evaluation that would preclude such cases, it is possible to determine a fraction of t_{ss} which should be compared to the cycle time period. Based on the analysis performed, the curves of Figure 9 indicate that for cycle times limited to 0.1 t_{ss}, contribution of creep rupture damage can be conservatively ignored in the failure analysis.

26
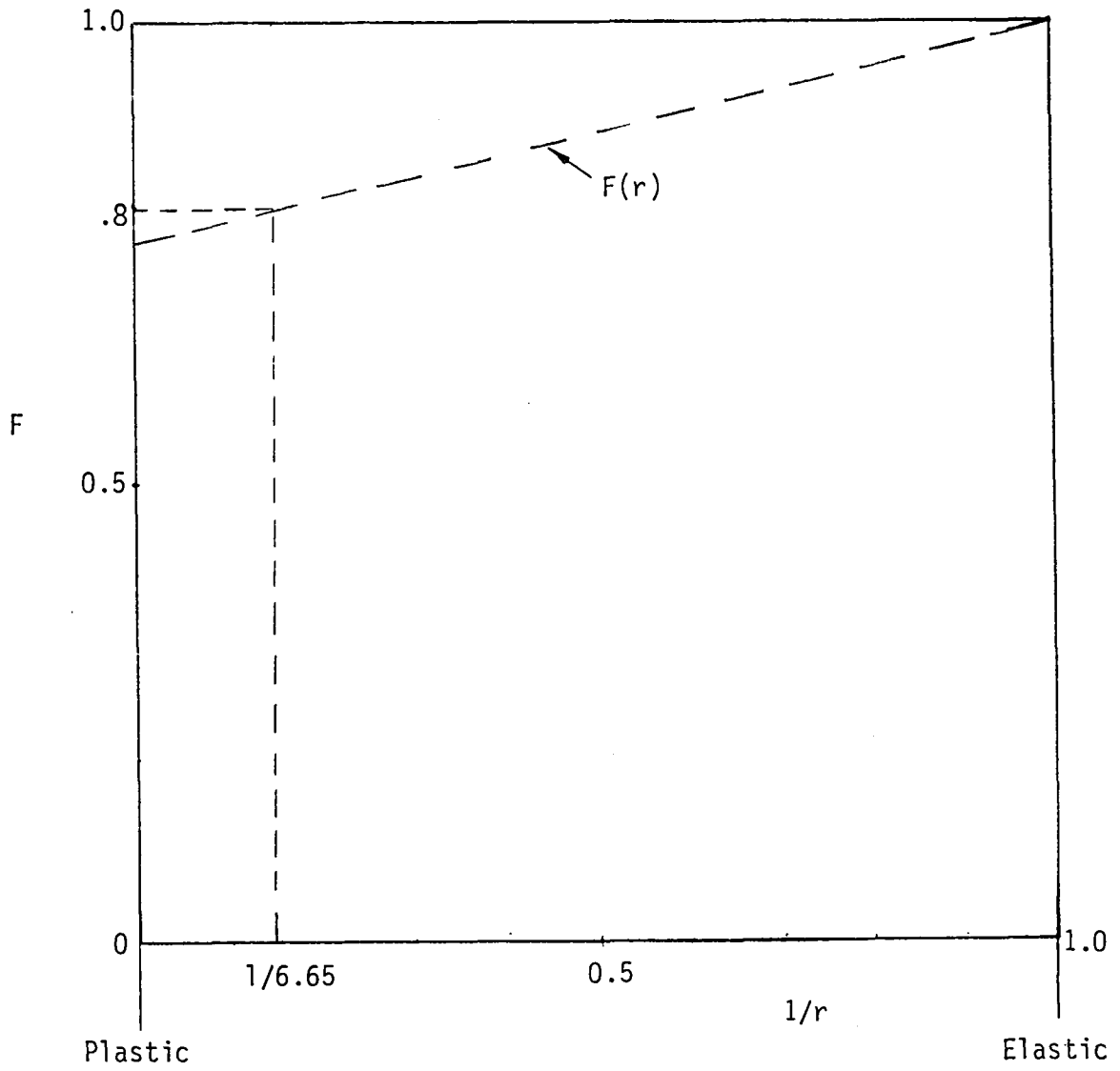
FIGURE 10   FACTOR F VS. 1/r

The creep rupture damage is determined from the stress to rupture curves. Since the thickness of the ligament changes with each cycle, a numerical procedure is used to evaluate the damage. Neglecting the effect of moment redistribution along the ligament, the initial pressure induced stress for each cycle is based on t_{min} from Equation (30). The total fatigue and creep rupture damage can be determined by linear summation, strain range partitioning or other damage summation methods.

Kachanov's creep rupture damage theory is described in Appendix A. If the stress rupture curve (log σ vs. log t_r) is not a straight line for a given temperature then damage accumulation will depend on the stress level and there could be a large deviation from unity if Robinson's life fraction rule is used in a linear manner [7]. Kachanov's theory can be useful in explaining such deviations. In the present case, either theory can be conveniently used for evaluating creep rupture damage.

3.3 Plastic Instability

At the peak of the heat transient, the ligament yields in compression. Thus, the stresses are compressive during the creep period. The ligament then yields in tension at the cold end of the cycle and ductile failure due to plastic tensile instability must be considered. The critical effective strain and critical ligament thickness were developed in [1] and are given by:

$$\bar{\varepsilon}_{cr} = \frac{2q(1-\alpha+\alpha^2)^{\frac{1}{2}}}{(2-\alpha)} \tag{34}$$

$$t_{cr} = 2He^{-q} \tag{35}$$

where $\alpha = \frac{\sigma_2}{\sigma_1}$ and σ_1 and σ_2 are the principal stresses in the hoop and axial directions, respectively.

28

4.0 THRUST CHAMBER LIFE PREDICTIONS

The analysis method developed herein provides the cyclic strains needed to perform a fatigue damage evaluation and the stresses needed to evaluate creep rupture damage. The latter is quite significant for the high pressures used in the SSME thrust chamber. The resulting combined damage may limit the life of the thrust chamber, i.e., the number of times it can be fired before ligament cracks can be anticipated. This analysis includes the effect of progressive geometry changes of the ligament on strain ranges and maximum stresses.

Plastic tensile instability is an independent mode of failure which is simultaneously checked with progressive deformation as an alternative possibility of failure. This mode of failure appears to be limiting for certain materials such as OFHC copper. NarloyZ appears to exhibit cyclic hardening mechanisms which when combined with corresponding shift of yield frame related to kinematic hardening results in gradually diminishing thinning in consecutive cycles. The interaction between creep hardening mechanisms and cyclic hardening is, of course, quite complex and beyond the scope of this evaluation. The present analysis does not take account for these complexities of material response and therefore may predict premature plastic tensile instability where such hardening is significant. Fatigue and creep rupture damage may, in fact, be more limiting than plastic tensile instability for NarloyZ.

The results obtained using the analyses described herein can be used for conservative estimates of the life of the thrust chamber. If the number of cycles to failure based on fatigue and creep rupture damage of the gradually thinned ligament are determined to be less than those needed to reduce the ligament thickness below the critical value resulting in plastic instability, then the failure mode is obvious and the cycles to failure due to fatigue and creep rupture damage correspond to the estimated life of the thrust chamber.

If, however, the number of cycles to reach the critical thickness obtained from the tensile instability analysis is determined to be less than that due to fatigue and creep rupture damage, then although the evaluation remains conservative the dominating failure mode for materials such as NarloyZ is not obvious. In these cases, plastic instability analysis and creep and fatigue damage evaluation provide lower and upper bounds on the cyclic life of the thrust chamber, respectively. Such situations may occur when the pressure differential across the ligament is low, as for example in test chambers but they are basically not expected for the SSME thrust chamber where the pressure differentials are substantially higher.

Numerical calculations for various cases of NarloyZ using the procedure developed herein are presented in Appendix B.

5.0 FINITE ELEMENT ANALYSES

A finite element model of the ligament was formulated to confirm the analytical procedure developed herein. The cross-hatched area in Figure 11 shows the ligament portion modeled. The finite element mesh along with the co-ordinate system and boundary conditions is shown in Figure 12. Two-dimensional isoparametric solid elements were used for the model. Assuming generalized plane strain conditions, the analysis was performed for NarloyZ using the thermal history obtained from [1] and shown here in Figure 13. The material was assumed to be elastic perfectly plastic and creep was allowed to occur for four minutes at the hot end of the cycle. Norton's law was used for the creep flow. The pressure load was taken as 3000 psi (20.68 MPa) and acted over the ligament portion shown in Figure 12.

The finite element mesh with the node numbers is shown in Figure 14. The results of the finite element analysis are shown in Figures 15 through 18. The stresses are plotted for nodes 133 to 143 which lie along the center-line of the ligament in the thickness or Y-direction. Sx is the hoop stress and SIGE is equivalent stress. Figure 15 shows the stresses due to a pressure of 3.000 psi (20.68 MPa). The thermal transient is then applied and the ligament yields compression, as illustrated in Figure 16. During creep, the hoop stress relaxes quite rapidly becoming tensile at the inside surface in about one second, as shown in Figure 17. Relaxation occurs to the steady state stress as shown in Figure 18.

The results for the high pressure case show that the stress is redis-tributed during creep and the steady state stress at the hot-gas-wall surface is approximately 80% of the initial value. Moreover, since the stress on the hot-gas-wall surface becomes tensile very rapidly compared to the cycle time, creep rupture damage is a potential failure mode that should be included in the failure analysis.
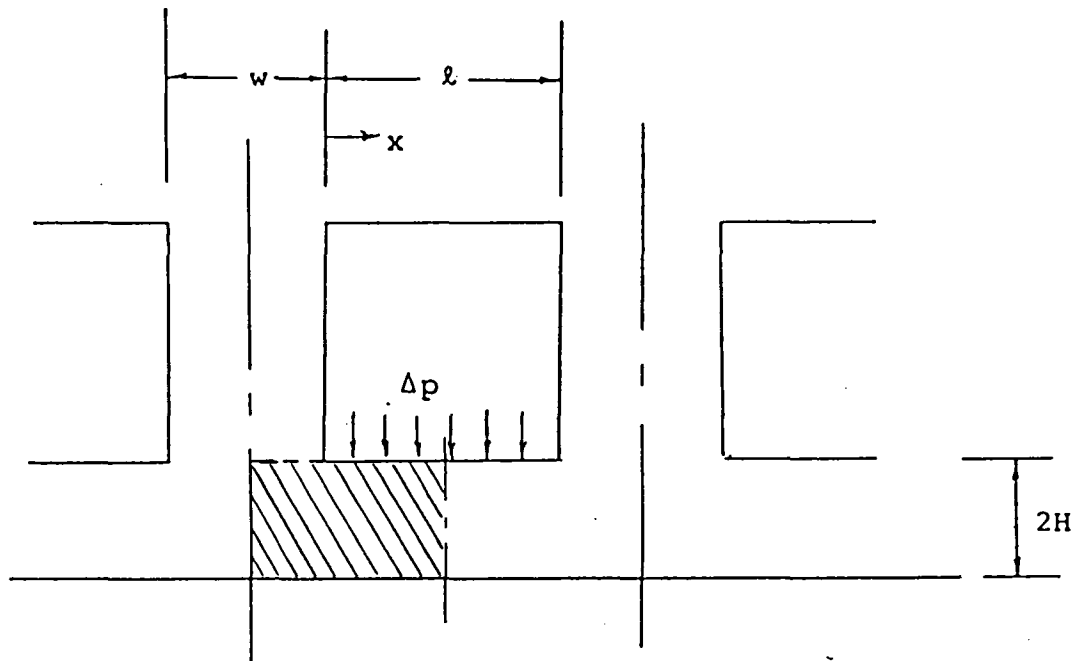
$$\ell = 0.0664" \quad (1.686 \text{ mm})$$

$$2H = 0.035" \quad (0.899 \text{ mm})$$

$$w = 0.05" \quad (1.27 \text{ mm})$$

FIGURE 11 LIGAMENT GEOMETRY
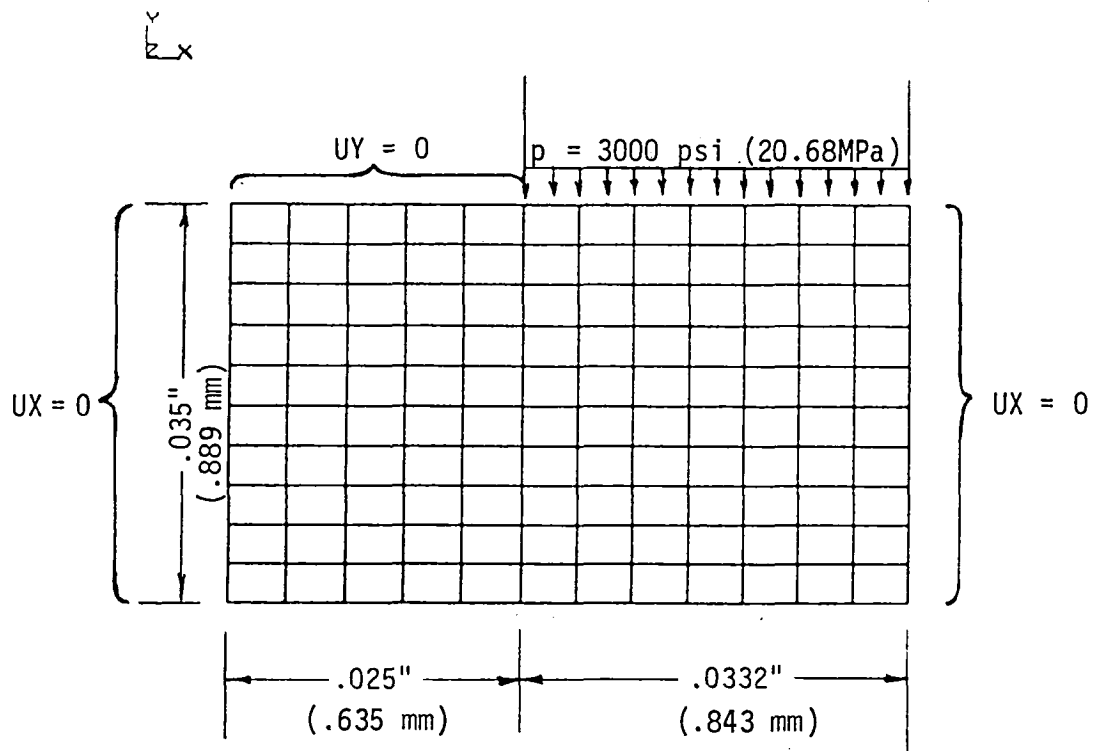
FIGURE 12 FINITE ELEMENT MODEL OF LIGAMENT

CURVE NO.   TIME (SEC.)
    1   =   1.45
    2   =   1.67
    3   =   1.7
    4   =   1.9
    5   =   3.2
    6   =   3.33
    7   =   3.45
    8   =   3.7
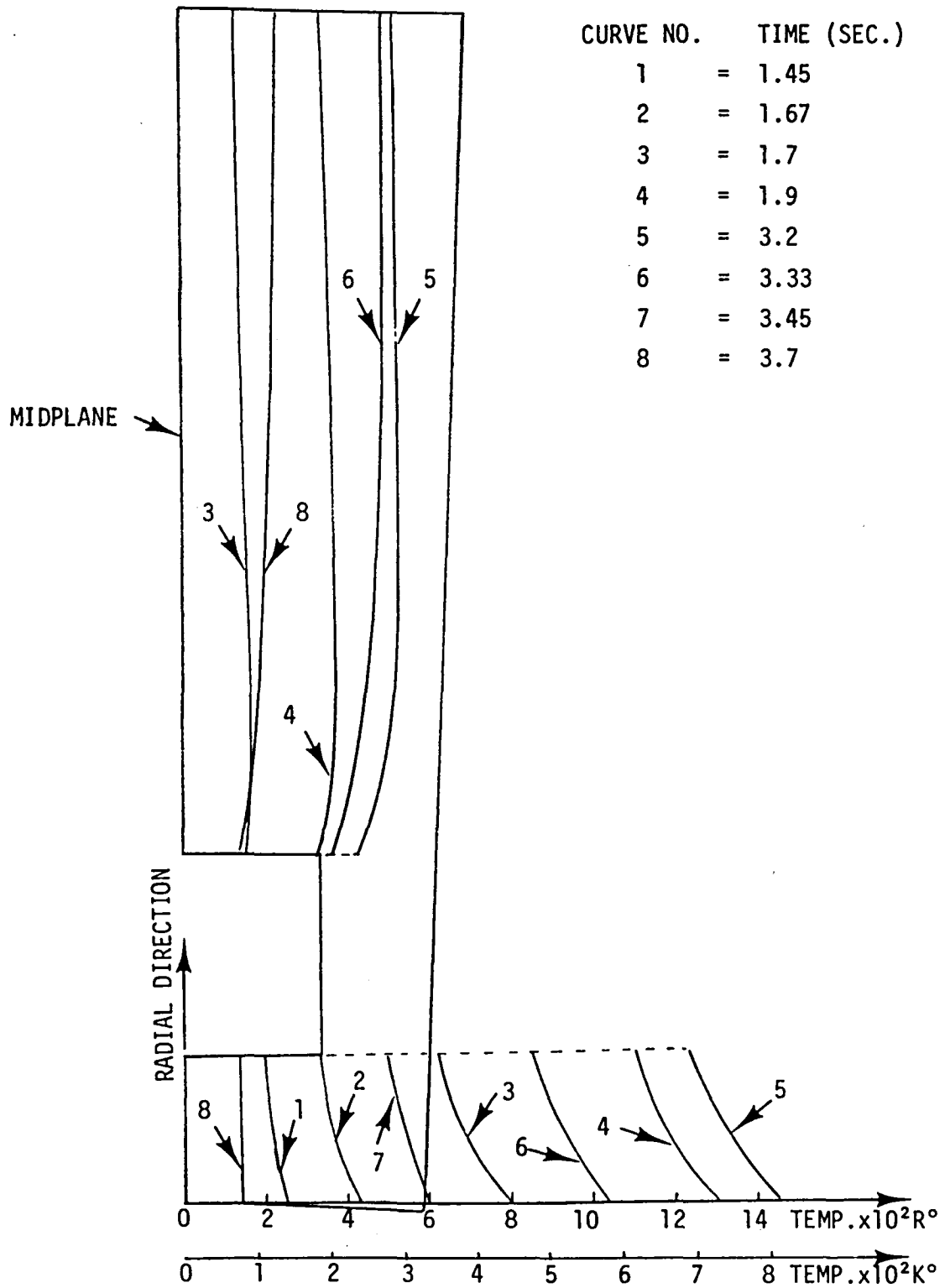
FIGURE 13   MIDPLANE TEMPERATURE HISTORY

Y
Z—X

w/2 ———— ℓ/2 ————

11	22	33	44	55	66	77	88	99	110	121	132	143
10	21	32	43	54	65	76	87	98	109	120	131	142
9	20	31	42	53	64	75	86	97	108	119	130	141
8	19	30	41	52	63	74	85	96	107	118	129	140
7	18	29	40	51	62	73	84	95	106	117	128	139
6	17	28	39	50	61	72	83	94	105	116	127	138
5	16	27	38	49	60	71	82	93	104	115	126	137
4	15	26	37	48	59	70	81	92	103	114	125	136
3	14	25	36	47	58	69	80	91	102	113	124	135
2	13	24	35	46	57	68	79	90	101	112	123	134
1	12	23	34	45	56	67	78	89	100	111	122	133

2H

S_x

Y

₵ OF RIB

₵ OF LIGAMENT

FIGURE 14   FINITE ELEMENT MESH WITH MODE NUMBERS

FIGURE 15 INITIAL CONDITION - P = 3000 PSI ONLY
(Y = 0 is Hot-gas-wall Surface)
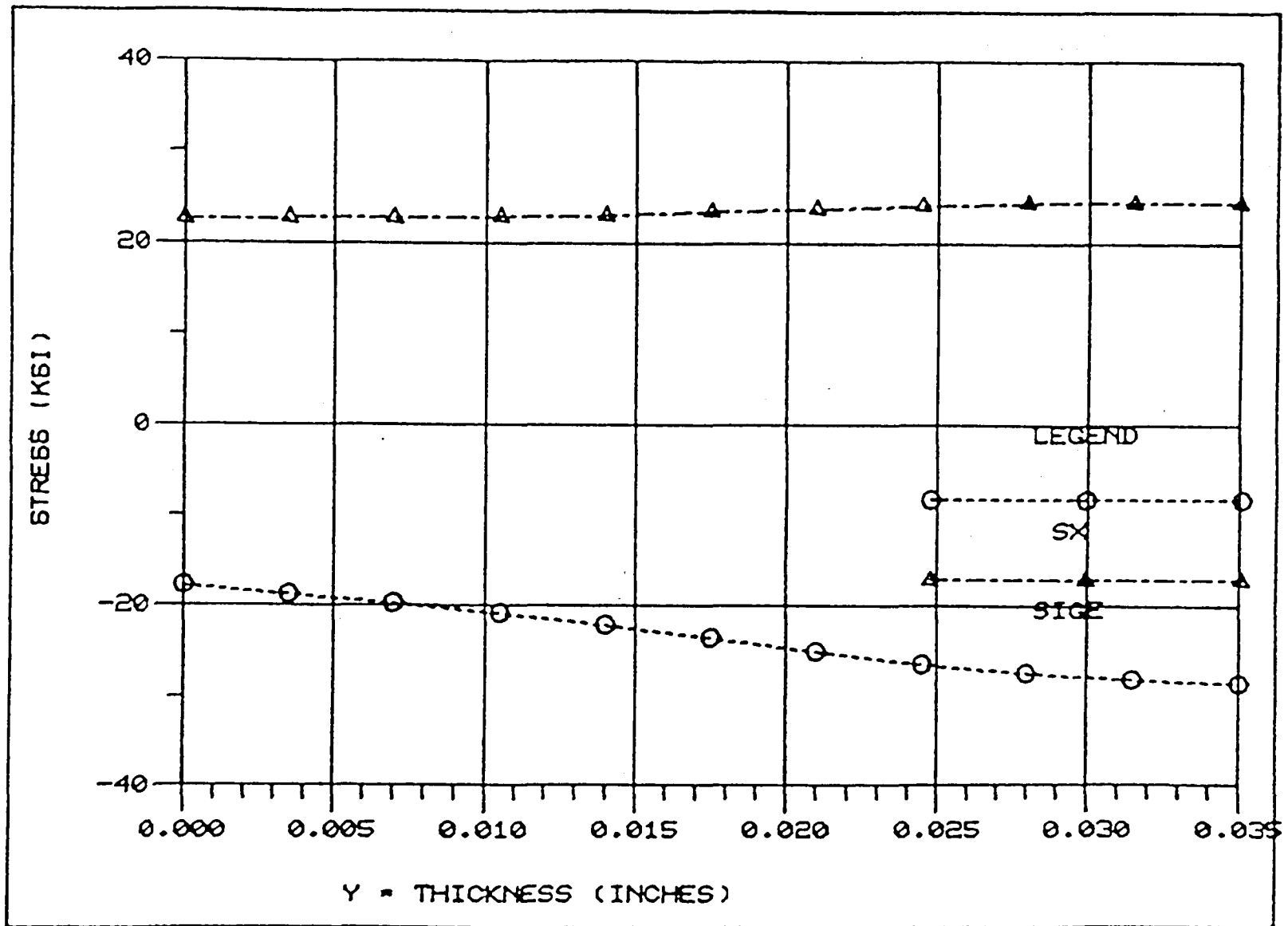
FIGURE 16   PEAK OF THERMAL TRANSIENT
(Y = 0 is Hot-gas-wall Surface)
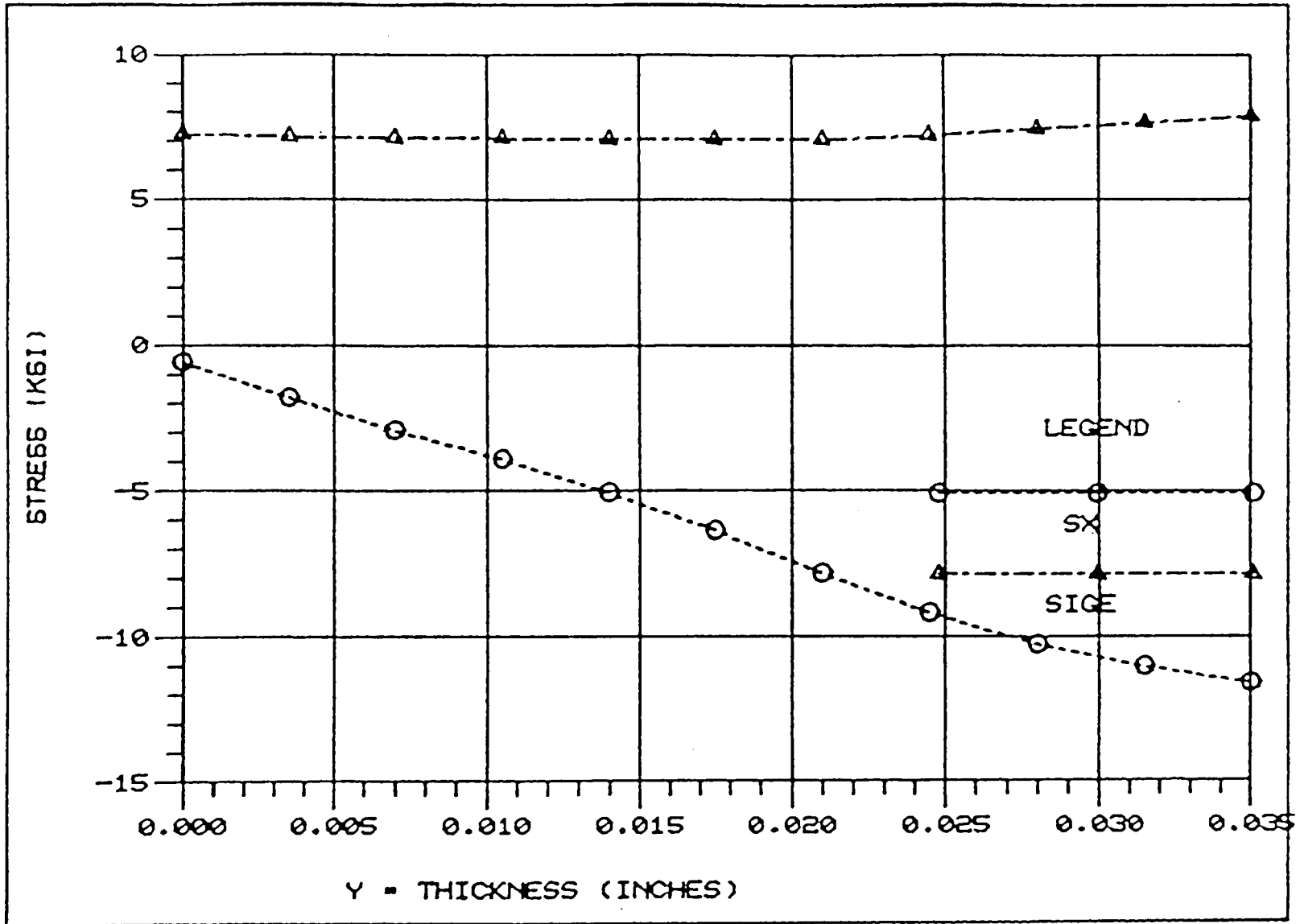
FIGURE 17   CREEP FOR ONE SECOND DURING THERMAL TRANSIENT - ΔT = 865°F
(Y = 0 is Hot-gas-wall Surface)
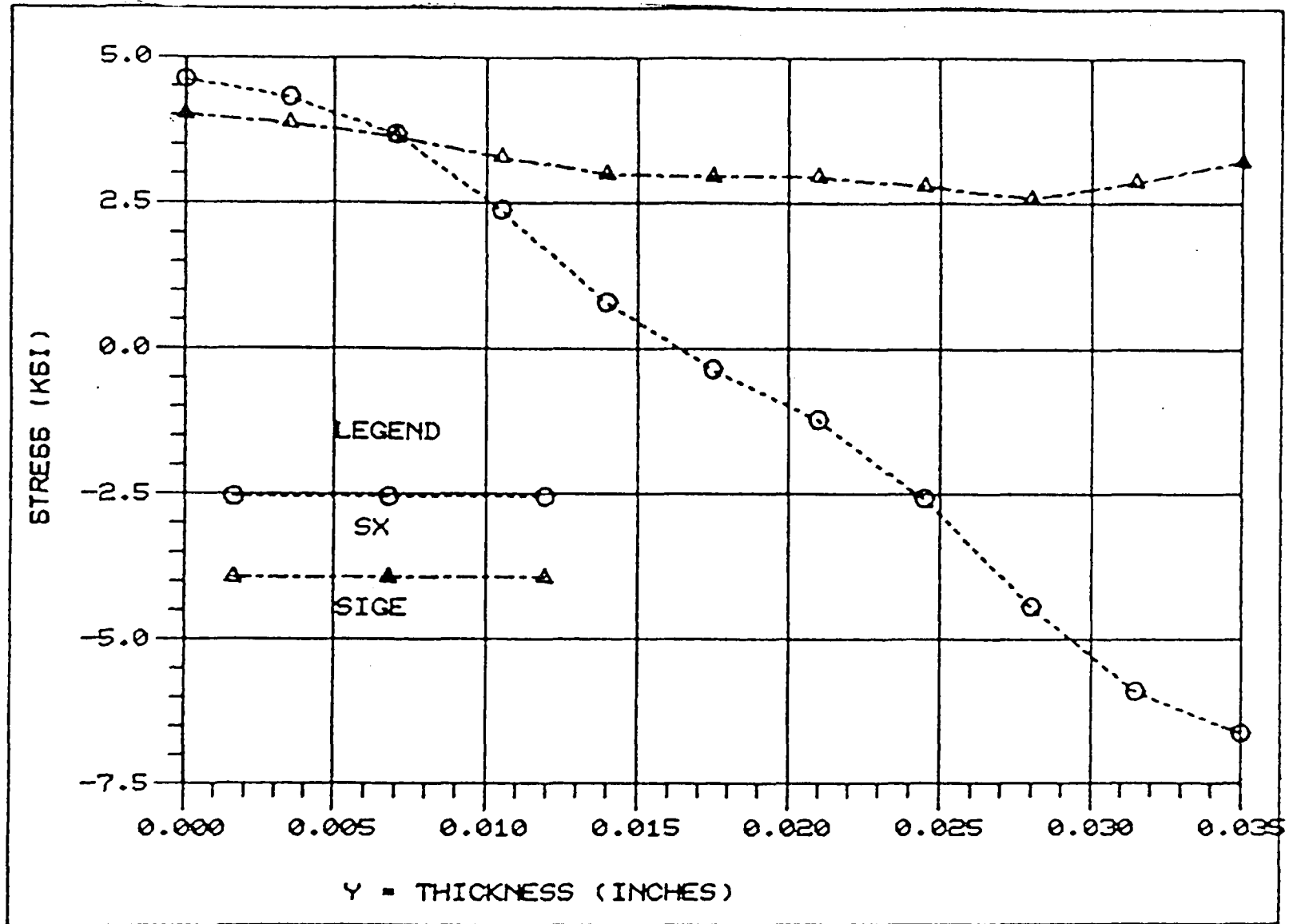
FIGURE 18 CREEP FOR 240 SECONDS DURING THERMAL TRANSIENT - ΔT = 865°F
(Y = 0 is Hot-gas-wall Surface)

To investigate if such is also the case with low pressures, a finite element analysis was performed for NARloy-Z using a pressure of 547 psi. (3.77 MPa). The finite element mesh, the model boundary conditions and the thermal history were the same as that for the high pressure case.

The results of this analysis are shown in Figures 19 through 21. The stresses are again plotted along the centerline of the ligament in the thickness or Y-direction. Figure 19 shows the stresses due to pressure only. Figure 20 shows the stresses at the peak of the transient. The ligament has yielded in compression. Figures 21 and 22 show the stresses after creep for one second and 240 seconds respectively. It is seen that there is negligible stress redistribution and the hoop stress remains compressive even after four minutes as compared to the previous case of high pressure (p = 3000 psi (20.68 MPa)) for which the hoop stress became tensile at the inside surface after only about one second.

The analysis for the low pressure case was then extended to include creep for eight minutes. It was found that the hoop stress remained compressive, indicating that creep rupture damage does not occur for low pressure cases.

The stress relaxation curves for the middle and inside ligament surface are plotted in Figures 3 and 9, respectively, for the two pressure cases analyzed.

The above analyses indicate that creep effects are significant for the SSME thrust chamber, and creep rupture damage should be considered since pressures are high. For the experimental thrust chamber, however, creep has little effect on the cycles to failure.
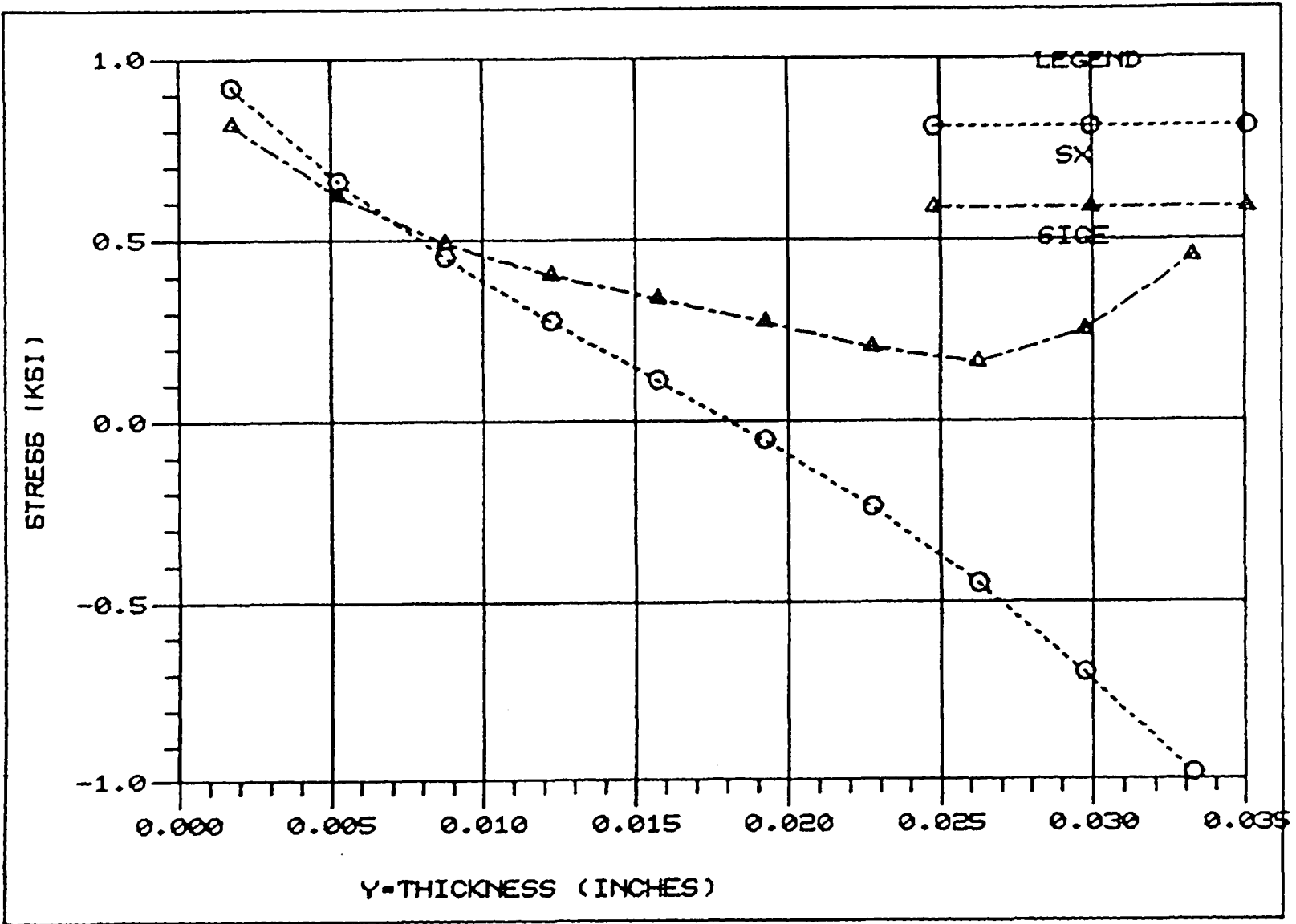
FIGURE 19 INITIAL CONDITION - P = 547 PSI ONLY
(Y = 0 is Hot-gas-wall Surface)
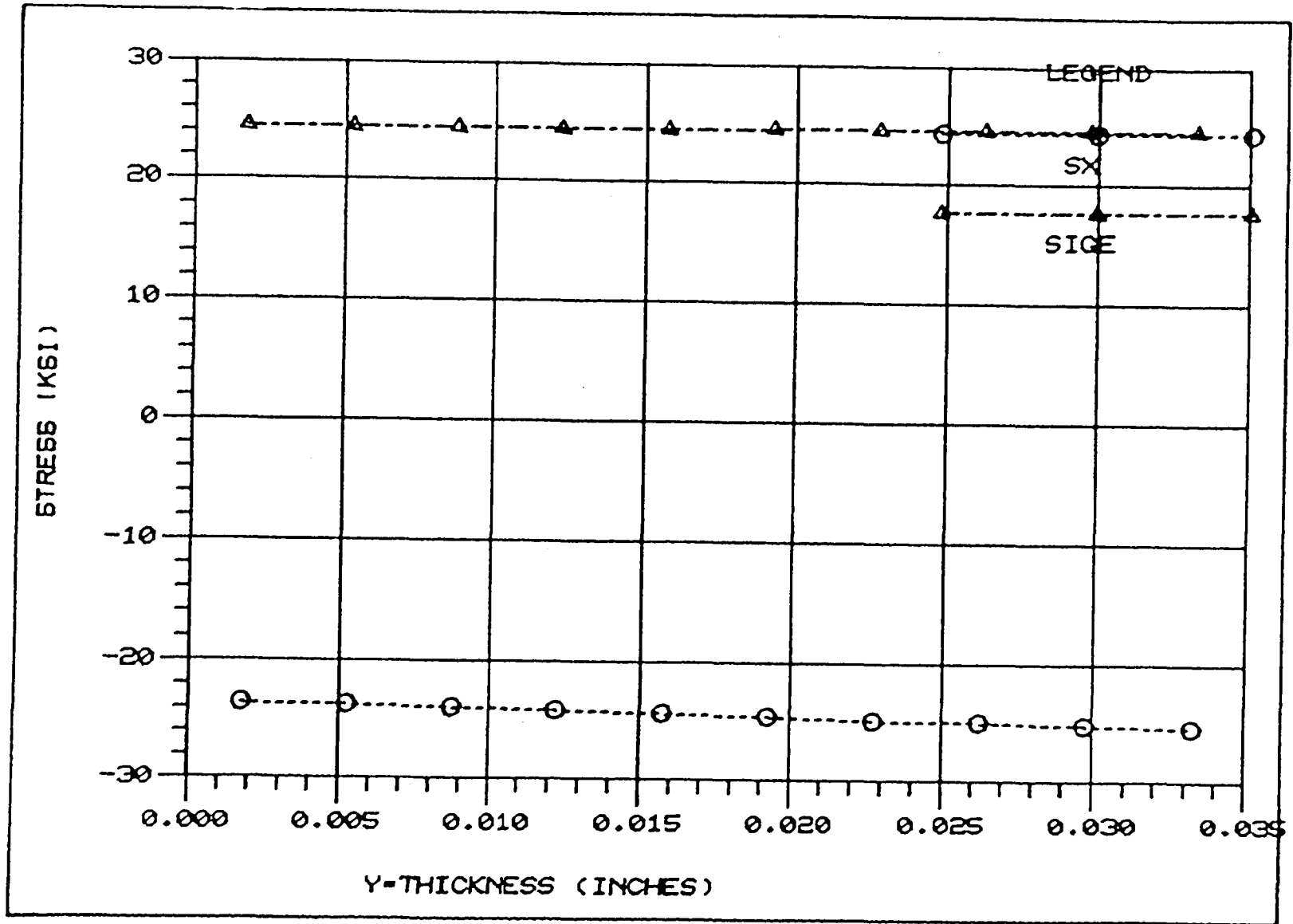
FIGURE 20   PEAK OF THERMAL TRANSIENT.
(Y = 0 is Hot-gas-wall Surface)
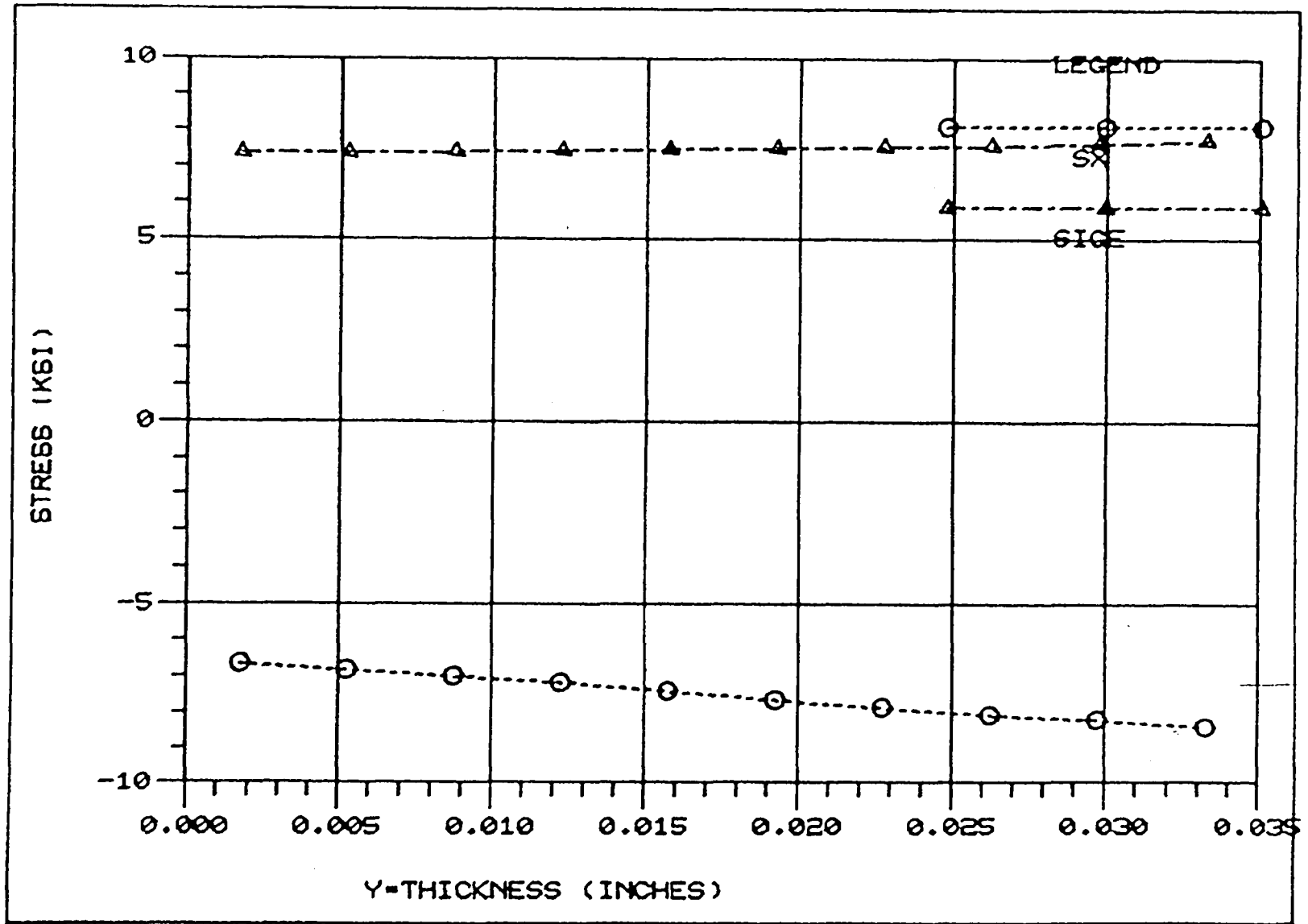
FIGURE 21 CREEP FOR ONE SECOND DURING THERMAL TRANSIENT - ΔT = 865°F
(Y = 0 is Hot-gas-wall Surface)
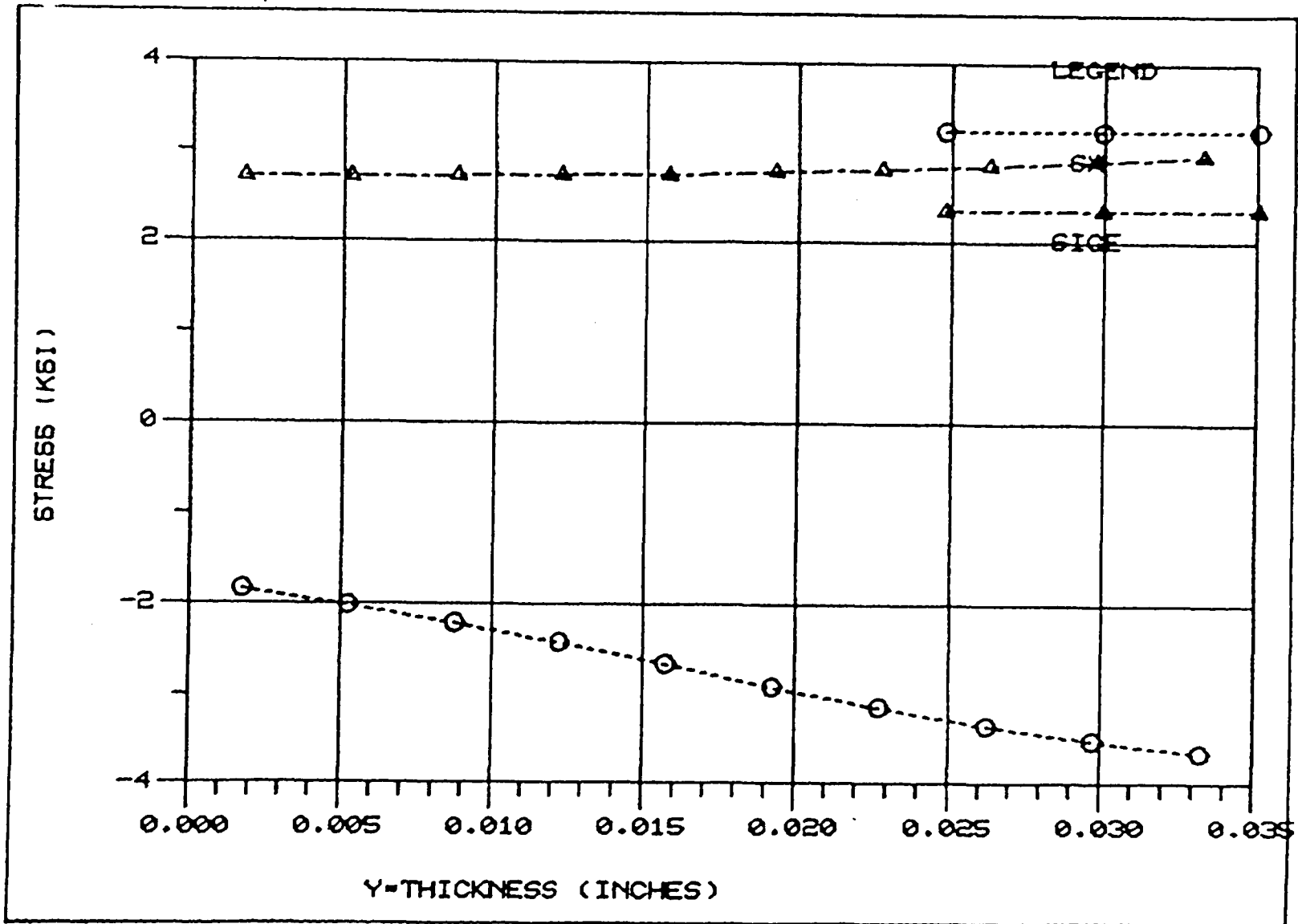
FIGURE 22 CREEP FOR 240 SECONDS DURING THERMAL TRANSIENT - ΔT = 865°F
(Y = 0 is Hot-gas-wall Surface)

6.0 COMPARISON OF RESULTS

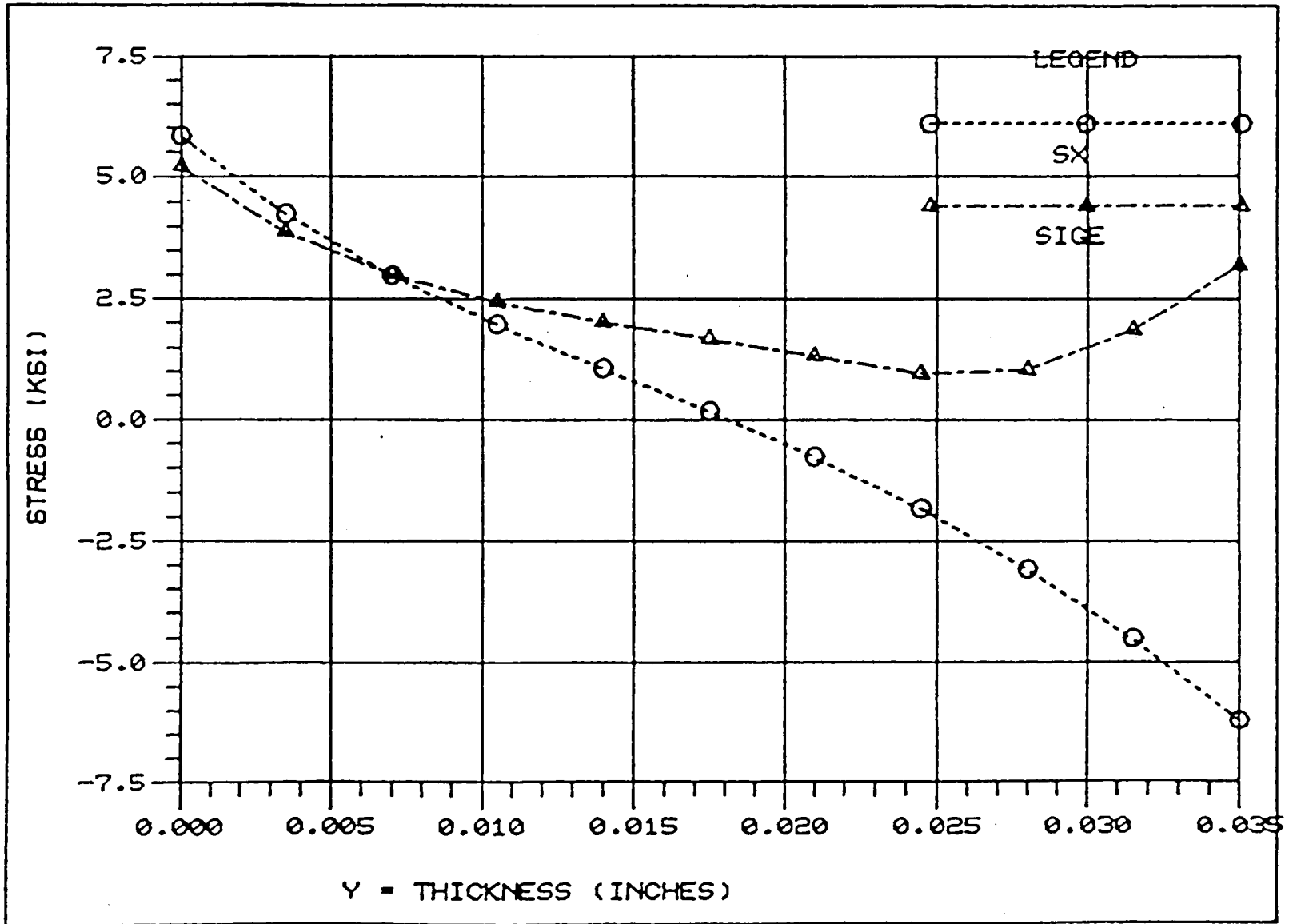The numerical results obtained using the analytical procedure developed herein are compared with the finite element results in Table II. The test case analyzed was the experimental thrust chamber geometry with a pressure differential of 3000 psi (20.68 MPa) corresponding to the SSME thrust chamber. The two are in very good agreement indicating that the analytical method is modeling the physical behavior of the ligament accurately.

TABLE II

COMPARISON OF ANALYTICAL VS. FINITE ELEMENTS RESULTS
Residual Deflection After One Cycle

Analytical Results	Finite Element Results
Deflection of Pressure Surface/Cycle	Deflection of Pressure Surface/Cycle
.34 mils (.0086mm)	.34 mils (.0086 mm)

7.0 CONCLUSIONS

An analytical method for predicting engine thrust chamber life is developed herein. The method accounts for high pressure differentials and time-dependent creep effects both of which are significant in limiting the useful life of the SSME thrust chamber.

It is demonstrated from the cases analyzed that when pressure differentials across the ligament are high, creep rupture damage is often the primary failure mode for the cycle times considered. It is therefore important that the thrust chamber is designed to minimize the combined stress and temperature effects on progressing creep damage of the material.

The simplified method of analysis developed herein provides the strain ranges and stresses needed to perform fatigue damage and creep rupture damage evaluations.

45

The simplifed method of analysis developed herein provides the number of firings which will result in a plastic tensile instability failure but takes no credit for the plastic and creep hardening mechanisms in materials such as NarloyZ. These hardening mechanisms have not been quantified* and may greatly extend the number of firings which may be tolerated prior to tensile instability.

The simplified method of analysis developed herein provides an excellent tool for making a parametric study to determine the coolant channel design and operating parameters which would maximize the number of repeated firings that could be achieved prior to failure.

---

*The relevant material properties could be measured on simple specimens but complex temperature and strain histories would have to be used in order to obtain the properties needed for analysis purposes.

8.0 REFERENCES

[1] "Development of a Simplified Procedure for Thrust Chamber Life Prediction," NASA CR-165585, Report prepared by O'Donnell & Associates, Inc. for NASA-Lewis under Contract NAS3-22649, October 1981.

[2] Hodge, P. G., Jr., "Plastic Analysis of Structures," McGraw Hill Book Co., 1959.

[3] Peterson, D. B., Kroenke, W. C., Stokey, W. F., O'Donnell, W. J., "Generalized Yield Surfaces for Plates and Shells," WRC Bulletin No. 250, July 1979.

[4] Anderson, R. G., Gardner, L. R.T, and Hodgkins, W. R., "Deformation of Uniformly Loaded Beams Obeying Complex Creep Laws," Journal of Mechanical Engineering Science, Vol. 5, No. 3, 1963.

[5] Calladine, C. R., "Time-Scales for Redistribution of Stress in Creep of Structures," Proc. Roy. SOC. A. 309, 1969.

[6] Calladine, C. R., "A Rapid Method for Estimating the Greatest Stress in a Structure Subjected to Creep," Proc. Instn, Mech. Engr., Vol. 178, 1963-64.

[7] Plumtree, A., "Creep/Fatigue Interaction in Type 304 Stainless Steel at Elevated Temperatures, Metal Science, August/September 1977.

KACHANOV'S BRITTLE CREEP RUPTURE DAMAGE THEORY

The usual approach to evaluating creep damage accumulation is based on Robinson's life fraction rule:

$$\sum_{i=1}^{N} \frac{t_i}{t_{ri}} = 1 \qquad\qquad (A-1)$$

where t_i is the time at a given stress level and t_{ri} is the rupture time for that stress. The concept implied in the model of Equation (A-1) is that damage accumulation is a linear process independent of the order of the succession of applied stress.

An alternative approach to evaluating brittle creep rupture damage is that due to Kachanov. His theory relates the damage rate to the maximum tensile stress in the current undamaged net area of the ligament cross-section. If A denotes the total cross-sectional area and A_r denotes the currently effective load carrying area, the creep rupture damage can be defined as:

$$D = \frac{A - A_r}{A} \qquad\qquad (A-2)$$

Kachanov postulated the following power relation for the creep damage rate:

$$\frac{dD}{dt} = C(\sigma_r)^\nu = C\left(\frac{\sigma}{1-D}\right)^\nu \qquad\qquad (A-3)$$

where σ and σ_r are the initial and current stresses corresponding to A and A_r, respectively, and C and ν are material constants. $D = 0$ corresponds to material in the virgin state and $D = 1$ corresponds to failure.

For a constant stress level, Equation (A-3) gives on integration:

$$\frac{-(1-D)^{\nu+1}}{\nu+1} = C\sigma^{\nu}t + \overline{K} \tag{A-4}$$

where $\overline{K}$ is the constant of integration.

Using the conditions that when $t = 0$, $D = 0$ and when $t = t_r$, $D = 1$ gives:

$$\overline{K} = -\frac{1}{\nu+1} \tag{A-5}$$

and

$$C\sigma^{\nu} = \frac{1}{t_r(\nu+1)} \tag{A-6}$$

Thus Equation (A-4) becomes

$$D = 1 - \left\{1 - \frac{t}{t_r}\right\}^{\frac{1}{\nu+1}} \tag{A-7}$$

If the plot of $\log \sigma$ vs $\log t_r$ for a given temperature is a straight line, then ν in Equation (A-7) is independent of the stress level and can be obtained from the slope of this line. In this case a single damage accumulation curve is obtained as shown schematically in Figure A-1 and the failure criterion is identical to the life fraction rule even though the damage accumulation process is nonlinear.

If the above condition does not hold for a particular temperature, then damage accumulation will depend on the stress level which in turn governs ν. When ν is stress-sensitive, there could be a large deviation from unity if the time ratio t/t_r is used in a linear manner, as illustrated in Figures A-2(a) and A-2(b). Kachanov's theory can be potentially useful in explaining these deviations in such situations.

In the present case, however, either theory can be conveniently used
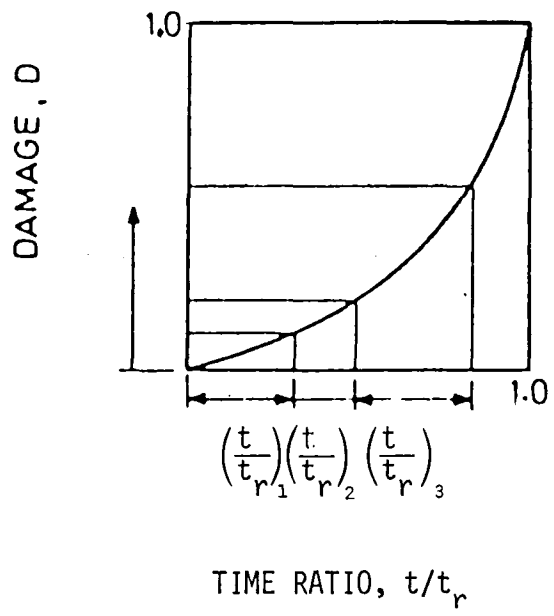
FIGURE A-1 DAMAGE VS. TIME RATIO WHEN ν
IS INDEPENDENT OF STRESS LEVEL

(a)

$\nu_1 < \nu_2$

$\sigma(\nu_1) < \sigma(\nu_2)$

Program: $\sigma_2 \rightarrow \sigma_1$

Result: $\sum_{i=1}^{2} \left(\frac{t}{t_r}\right)_i > 1$

(b)

Program: $\sigma_1 \rightarrow \sigma_2$

Result: $\sum_{i=1}^{2} \left(\frac{t}{t_r}\right)_i < 1$
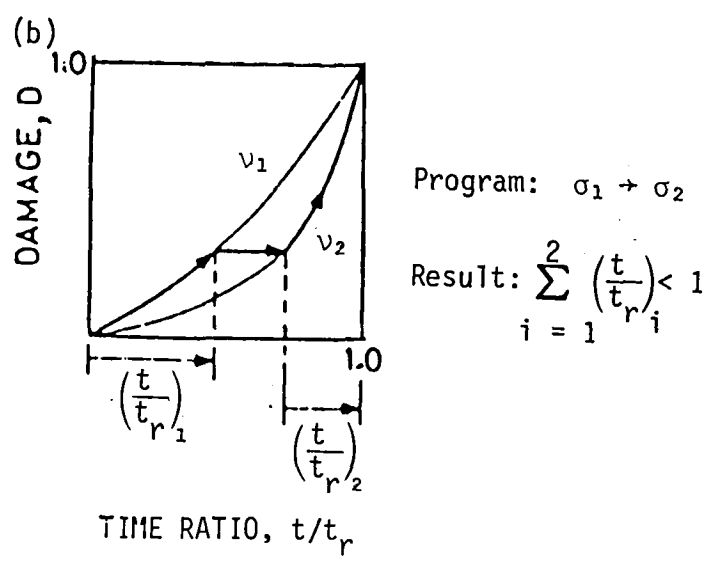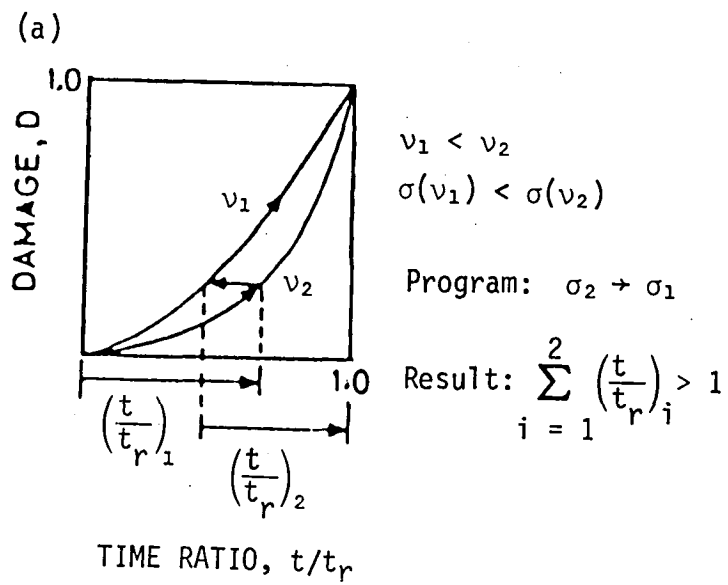
FIGURE A-2   DAMAGE VS. TIME RATIO   WHEN ν IS
DEPENDENT ON STRESS LEVEL

51

to evaluate the creep rupture damage, the two being related through
Equation (A-7). Figure A-3 is a schematic illustration of D representing
the area damage using Kachanov's theory and t/t_r representing the linear
damage theory vs. cycle ratio. This figure graphically illustrates the
physical difference between these two theories.
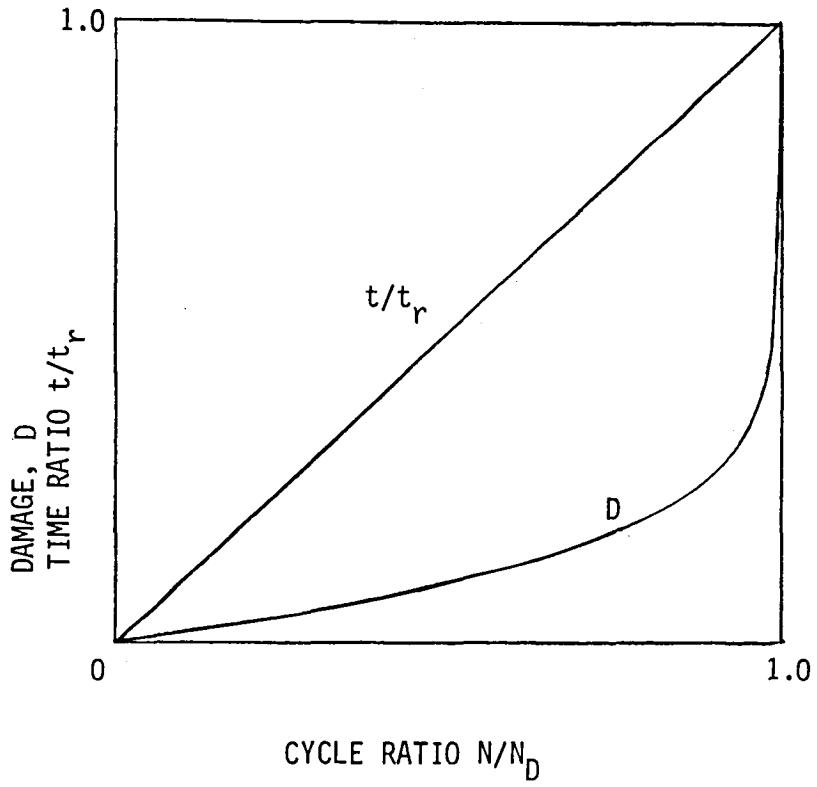
FIGURE A-3 SCHEMATIC VARIATION OF D and t/t_r VS CYCLE RATIO

APPENDIX B

NUMERICAL EXAMPLES

Example I:

Consider the ligament geometry shown in Figure B-1. The material is NARloy Z, with the following properties:

Yield Stress S_y = 24,500 psi
Young's Modulus E = 16.35 x 10^6 psi
Poisson's Ratio ν = 0.34
Coefficient of Thermal Expansion, α = 9.5 x 10^{-6} in/in°F

For a unit width of the ligament Δp = 3000 lb/in.
From Equation (1), taking $\alpha_i = \alpha_o = \alpha$ and $\left(S_{y_{max}} + S_{y_{min}}\right)/2 = S_y$, gives the inelastic strain range due to differential thermal expansion and creep relaxation:

$$\Delta \varepsilon'_{p_1} = \left[\alpha \left\{ \left(T_i - T_o\right)_{max} - \left(T_i - T_o\right)_{min} \right\} - \frac{2S_y}{E}\right] + \frac{\Delta\sigma_c}{E} \qquad (B-1)$$

From thermal analysis:

$$\left|\left(T_i - T_o\right)_{max} - \left(T_i - T_{o\ min}\right)\right| \approx 865°F$$

Creep law:

$$\dot{\varepsilon} = B\sigma^r$$

The ligament temperature was taken to be 1325°F, with the following creep constants estimated from Table B-1:

B = 5.5225 x 10^{-7}
r = 6.65

and σ is in ksi.

54
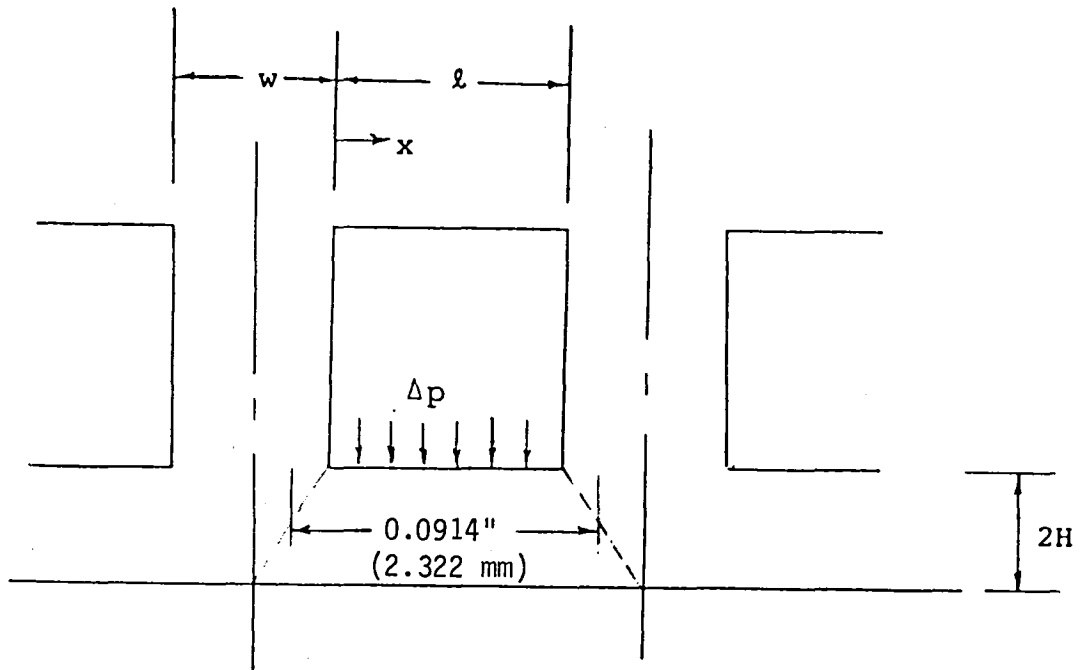
FIGURE B-1 LIGAMENT GEOMETRY

$\ell = 0.0664"$ (1.686 mm)

$2H = 0.035"$ (0.889 mm)

$w = 0.05"$ (1.27 mm)

TABLE B-1

Creep Constants for NARloy Z

TEMP.	r	B
700F (371.1°C)	19.2	2.9×10^{-31}
800F (426.7°C)	16.1	9.6×10^{-25}
900F (482.2°C)	13.9	1.0×10^{-19}
1000F (537.8°C)	12.5	6.2×10^{-16}
1200F (648.9°C)	8.7	4.5×10^{-9}
1500F (815.6°C)	4.6	1.1×10^{-6}

The mid-plane stress relaxes to almost zero as seen from Figure 3. Thus from Equation (8)

$$\Delta\sigma = S_y = 24,500 \text{ psi}$$

From Equation (B-1)

$$\Delta\varepsilon'_{p_1} = \left[9.5 \times 10^{-6} \times 865 - \frac{2 \times 24500}{16.35 \times 10^6}\right] + \frac{24500}{16.35 \times 10^6}$$

$$= 0.006719$$

The temperature drop across the ligament $\Delta T \approx 210°F$. Thus from Equation (2) the correction to the plastic strain range due to thermally induced bending:

$$\Delta\varepsilon''_{p_1} = \frac{16.35 \times 10^6 \times (9.5 \times 10^{-6} \times 210)^2}{12(1 - 0.34)^2 \times 24500}$$

$$= .000508$$

From Equation (3), total inelastic strain

$$\varepsilon_1 = 2(.006719 + .000508)$$
$$= .014454$$

From Equation (16), taking $n \approx k$ gives:

$$K = \frac{1}{R} = \frac{\varepsilon_1}{H}$$

where the radius R is assumed for the length shown in Figure B-2

Thus

$$R = \frac{.0175}{.014454} = 1.211"$$
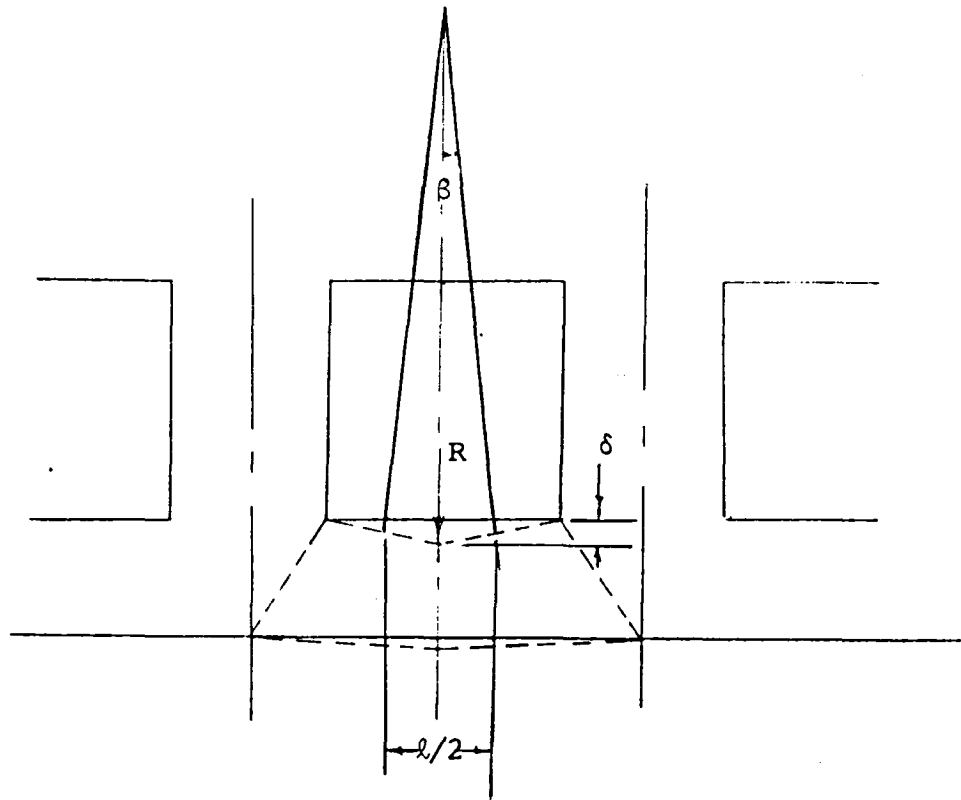
FIGURE B-2   DEFORMED LIGAMENT

Deflection $\delta_1 = 2R(1 - \cos\beta)$

$$= 2(1.211)[1 - \left\{(1.211)^2 - (.0166)^2\right\}^{\frac{1}{2}}/1.211]$$

$$= .0002276"$$

Equation (17) is approximated by:

$$\gamma = 2s\epsilon_1 \qquad\qquad\qquad\qquad \text{(B-2)}$$

where the dimensionless shear stress s is given by [1]:

$$s = \frac{p}{HS_y} \left(\frac{\ell}{2} - x\right)$$

Thus, $s = \dfrac{3000}{.0175 \times 24500} \left(\dfrac{.0664}{2} - x\right)$

$$= .2323 - 6.9971x$$

Substituting in Equation (B-2) integrating and determining the shear deflection at $x = \ell/2$ due to pressure loading, gives

$$\delta_2 = .000112$$

From Table I, for $r = 6.65$, $\overline{F}(r) = .1168$ by linear interpolation

Thus from Equation (24) for cycle time $t = .0667$ hr (4 min) and pressure of 3 ksi, the creep-induced deflection:

$$\delta_3 = \frac{5.5225 \times 10^{-7} \times .0667 \times (.0664)^2}{4 \times .0175} \left(\frac{3 \times .0664^2}{16 \times .0175^2}\right)^{6.65} \times .1168$$

$$= .0000002"$$

Thus total $\delta = \delta_1 + \delta_2 + \delta_3$

$$= .0003398"$$

From Equation (26), thinning after N cycles:

$$t_N = \frac{.0003398 \times .05N}{(.0664 + .05)}$$

$$t_N = .000146 \ N \text{ inches} \qquad\qquad (B-3)$$

Plastic Instability:

The strain hardening parameter q is approximately given by LeRc as

$$q = 0.2 \left(\frac{S_u - S_y}{S_y}\right)^{0.6}$$

For S_u = 55 ksi and S_y = 24.5 ksi

$$q = 0.2 \left(\frac{55 - 24.5}{24.5}\right)^{0.6} = .228$$

From Equation (35)

$$t_{cr} = (.035)e^{-0.228}$$

$$= .02786$$

$$\text{Thinning for instability} = .035 - .02786 \qquad\qquad (B-4)$$
$$= .00714"$$

Equating (B-3) and (B-4)

N = 49 cycles.

Fatigue and Creep Rupture Damage

The procedure of section 3.0 was used for evaluating fatigue and creep rupture damage. The fatigue curve of Figure B-3 and the stress to rupture curve of Figure B-4 were used as the basis of this evaluation. Linear summation was employed to estimate total damage.

60
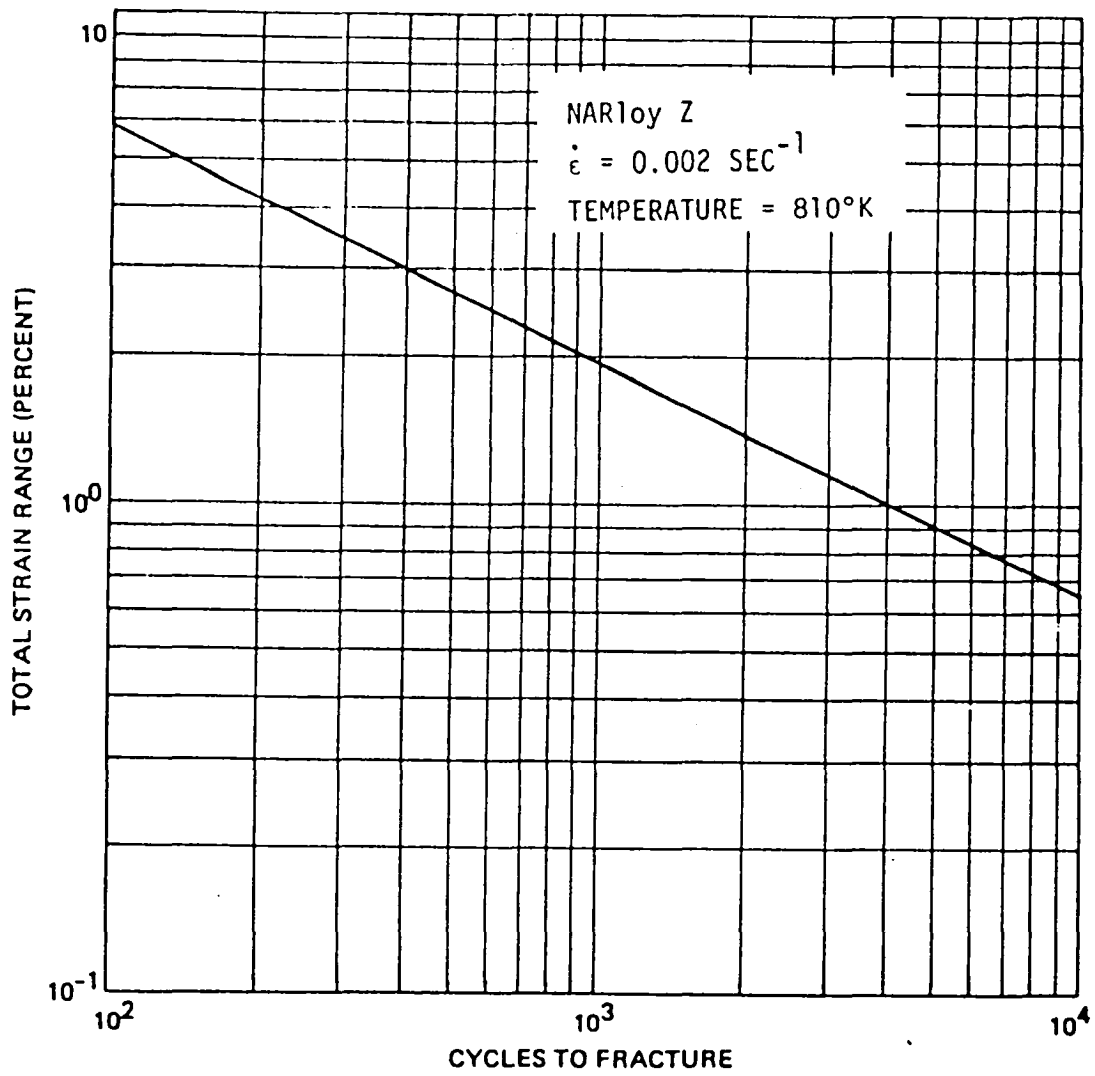
FIGURE B-3   TYPICAL LOW-CYCLE FATIGUE LIFE OF NARloy Z
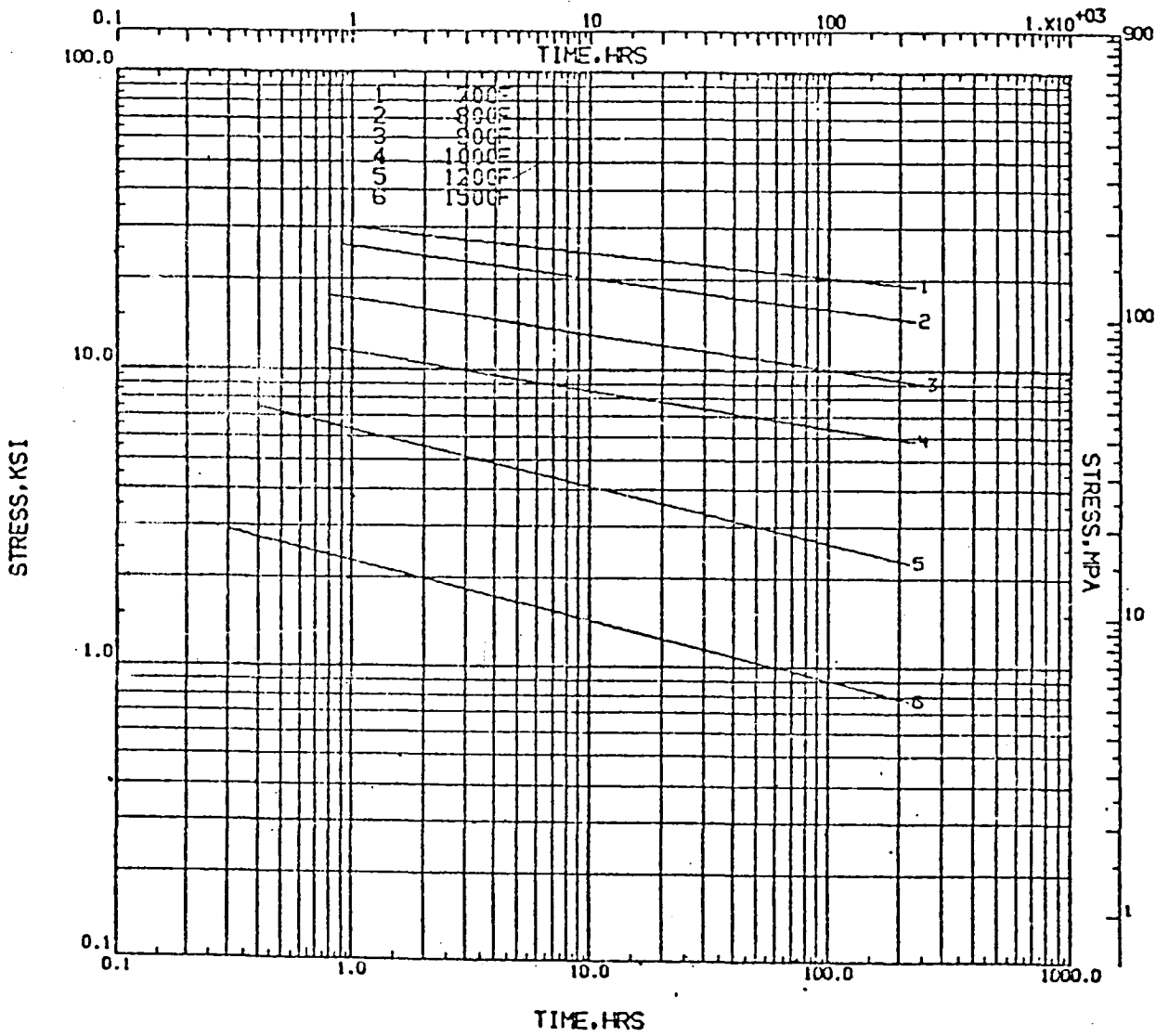
FIGURE B-4   STRESS TO RUPTURE CURVES FOR NARloy Z

From Figure 10, for r = 6.65, factor F = 0.8. Thus from Equation (33) the steady state stress:

$$\sigma_{ss} = 0.8\ \sigma_{in} \tag{B-5}$$

The initial stress is estimated by treating the ligament as a clamped beam under pressure loading. From Figure B-1 the mid-surface length of the beam = 0.0914". For simplicity and conservatism, the loading is assumed to be over this engire length.* Thus

$$\sigma_{in} = \frac{3000\ (.0914)^2}{4(.035)^2} = 5115\ \text{psi}$$

From Equation (B-5) σ_{ss} = 0.8 x 5115 = 4092 psi

Substituting in Equation (32)

$$t_{ss} = \frac{1}{5.225 \times 10^{-7} \times (4.092)^{6.65}} \times \frac{2.3}{6.65} \times \frac{5.115}{16.35 \times 10^3}$$

$$= .\ 0167\ \text{hrs.} = 60\ \text{seconds}$$

The creep constants for 1325°F were used in the finite element analysis and hence are also used here in evaluating t_{ss}. Since 0.1 t_{ss} is less than the creep period of four minutes, creep rupture damage is based on $\dot{\sigma}_{ss}$. The FORTRAN program listed in Appendix C was used for performing the necessary calculations. The input and output obtained are enclosed in this Appendix.

The notation for the listed results is as follows:

NCYC - Number of cycles
TMIN - t_{min}, minimum ligament thickness - in.

---

*Assuming a .0914" long beam that is loaded over a partial length of ℓ = 0664" gives a slightly lower stress.

TMAX - t_{max}, maximum ligament thickness - in.

EEQVT - effective strain range %

N/N_D - fatigue damage

STRESS- primary stress due to pressure

T/T_D - creep rupture damage

TOTAL USEAGE - cumulative usage factor

NF CYCLES - cycles to failure

The output shows that since T/T_D is substantially higher than N/N_D, creep rupture damage is the dominating failure mode, fatigue being negligible. The estimated life is determined to be nine cycles.

CONSTANTS INPUT

Q= 0.22800

DELTA = 0.33980E-03 INCHES

E1AVG = 0.82175   PERCENT

H = 0.17500E-01 INCHES

L = 0.66400E-01 INCHES

W = 0.50000E-01 INCHES

P = 3000.0   LBS/INCH

T/CYC = 4.0000   MINUTES

SF = 0.80000

FATIGUE CURVE

CYCLES	STRAIN RANGE
10.000	18.000
100.00	5.9000
4000.0	1.0000
0.50000E+06	0.10000E+00

STRESS-TO-RUPTURE CURVE

HOURS	STRESS (KSI)
0.10000E+00	6.0000
0.80000	4.0000
8.0000	2.5000
100.00	1.5000
1000.0	1.0000

RESULTS FOR EACH CYCLE

NCYC	TMIN	TMAX	EEQVT	N/NO	STRESS	T/TD	TOTAL USAGE	NF CYCLES
1	0.34854E-01	0.35083E-01	1.6554	0.71265E-03	4.1261	0.97710E-01	0.98422E-01	10
2	0.34708E-01	0.35167E-01	1.6675	0.72352E-03	4.1609	0.10201	0.20115	9
3	0.34562E-01	0.35250E-01	1.6798	0.73464E-03	4.1961	0.10651	0.30840	9
4	0.34416E-01	0.35333E-01	1.6922	0.74603E-03	4.2317	0.11124	0.42039	9
5	0.34270E-01	0.35416E-01	1.7049	0.75769E-03	4.2679	0.11620	0.53734	8
6	0.34124E-01	0.35500E-01	1.7178	0.76963E-03	4.3045	0.12140	0.65951	8
7	0.33978E-01	0.35583E-01	1.7309	0.78187E-03	4.3415	0.12685	0.78714	8
8	0.33832E-01	0.35666E-01	1.7442	0.79440E-03	4.3791	0.13258	0.92051	8
9	0.33686E-01	0.35749E-01	1.7577	0.80723E-03	4.4171	0.13859	1.0599	8

Example II

Consider the ligament geometry shown in Figure B-6 which corresponds to that of the SSME thrust chamber. The material is NARloy Z, with the following properties:

Yield Stress S_y = 24,500 psi

Young's Modulus E = 16.35 x 10⁶ psi

Poisson's Ratio ν = 0.34

Coefficient of Thermal Expansion, α = 9.5 x 10⁻⁶ in/in°F

For a unit width of the ligament Δp = 3000 lb/in.

From Equation (1), taking $\alpha_i = \alpha_o = \alpha$ and $\left(S_{y_{max}} + S_{y_{min}}\right)/2 = S_y$, gives:

$$\Delta \varepsilon'_{p_1} = \left[\alpha \left\{ \left(T_i - T_o\right)_{max} - \left(T_i - T_o\right)_{min}\right\} - \frac{2S_y}{E}\right] + \frac{\Delta\sigma_c}{E} \qquad (B-1)$$

From thermal analysis, for 120% power level,

$$\left\{\left(T_i - T_o\right)_{max} - \left(T_i - T_{o\ min}\right)\right\} \approx 1500°F$$

Creep law:

$$\dot{\varepsilon} = B\sigma^r$$

For an average ligament temperature of 1000°F, the creep constants from Table B-1 are:

B = 6.2 x 10⁻¹⁶

r = 12.5

and σ is in ksi.

67
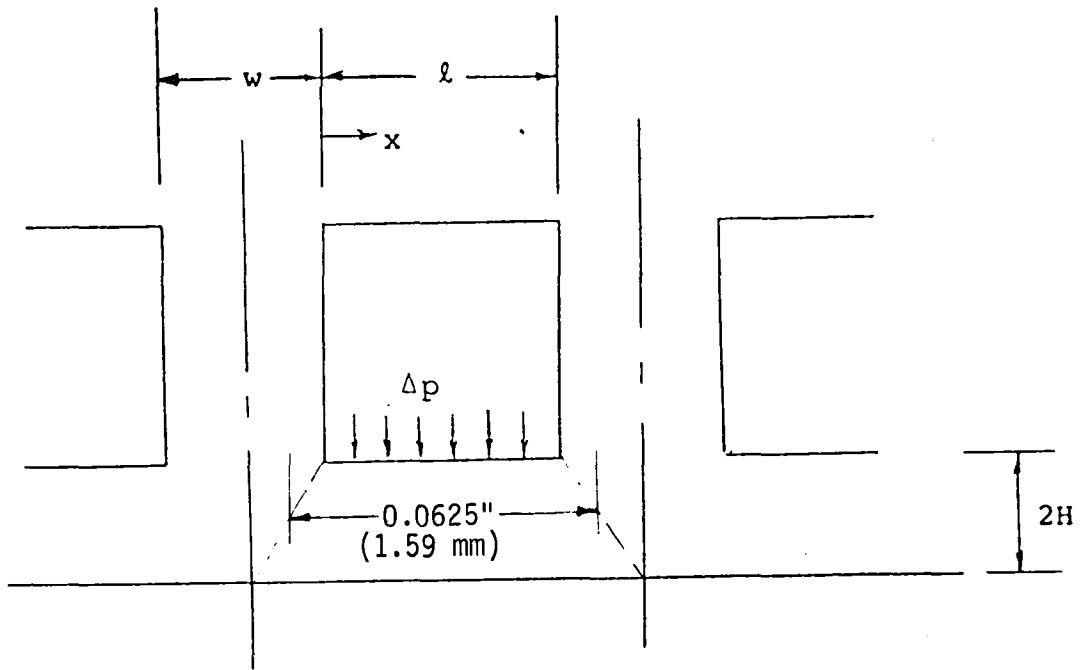
$$\ell = 0.04"\quad (1.016 \text{ mm})$$

$$2H = 0.028"\quad (0.711 \text{ mm})$$

$$w = 0.045"\quad (1.143 \text{ mm})$$

FIGURE B-6   LIGAMENT GEOMETRY

The mid-plane stress relaxes to almost zero. Thus from Equation (8)

$$\Delta\sigma = S_y = 24{,}500 \text{ psi}$$

From Equation (B-1)

$$\Delta\epsilon'_{p_1} = \left[9.5 \times 10^{-6} \times 1500 - \frac{2 \times 24500}{16.35 \times 10^6}\right] + \frac{24500}{16.35 \times 10^6}$$

$$= 0.0127515$$

The temperature drop across the ligament $\Delta T \approx 650°F$. Thus from Equation (2):

$$\Delta\epsilon''_{p_1} = \frac{16.35 \times 10^6 \times (9.5 \times 10^{-6} \times 650)^2}{12(1 - 0.34)^2 \times 24500}$$

$$= 0.0048681$$

From Equation (3), total inelastic strain

$$\epsilon_1 = 2(.0127515 + .0048681)$$
$$= .0352391$$

From Equation (16), taking $n \approx k$ gives:

$$K = \frac{1}{R} = \frac{\epsilon_1}{H}$$

where the radius R is assumed for the length shown in Figure B-2

Thus

$$R = \frac{.014}{.0352391} = .03973"$$

Deflection $\delta_1 = 2R(1 - \cos\beta)$

$$= 2(.3973)[1 - \left\{(.3973)^2 - (.01)^2\right\}^{\frac{1}{2}}/.3973]$$

$$= .0002517"$$

Equation (17) is approximated by:

$$\gamma = 2s\epsilon_1 \qquad\qquad (B-2)$$

where $\qquad s = \dfrac{p}{HS_y}\left(\dfrac{\ell}{2} - x\right)$

Thus, $s = \dfrac{3000}{.014 \times 24500}\left(\dfrac{.04}{2} - x\right)$

$$= .1749 - 8.7464x$$

Substituting in Equation (B-2) integrating and determining the deflection at $x = \ell/2$ gives

$$\delta_2 = .0001233$$

From Table I, for $r = 6.65$, $F(r) = .1168$

Thus from Equation (24) for cycle time $t = .0667$ hr.

$$\delta_3 = \frac{6.2 \times 10^{-16} \times .0667 \times (.04)^2}{4 \times .014}\left(\frac{3 \times .04^2}{16 \times .014}\right)^{6.65} \times .1168$$

$$\approx 0$$

Thus total $\delta = \delta_1 + \delta_2 + \delta_3$

$$= .000375"$$

70

From Equation (26), thinning after N cycles:

$$t_N = \frac{.000375 \times .045N}{(.04 + .045)}$$

$$t_N = .0001985N \text{ inches} \tag{B-3}$$

Plastic Instability:

For S_u = 55 ksi and S_y = 24.5 ksi

$$q = 0.2 \left(\frac{S_u - S_y}{S_y}\right)^{0.6}$$

$$q = 0.2 \left(\frac{55 - 24.5}{24.5}\right)^{0.6} = .228$$

From Equation (35)

$$t_{cr} = (.028)e^{-0.228}$$

$$= .0222915$$

$$\text{Thinning for instability} = .028 - .0222915 \tag{B-4}$$

$$= .0057085$$

Equating (B-3) and (B-4)

N = 29 cycles.

Fatigue and Creep Rupture Damage

The procedure of section 3.0 was used for evaluating fatigue and creep rupture damage. The fatigue curve of Figure B-3 and the stress to rupture curve of Figure B-4 were used as the basis of this evaluation. Linear summation was employed to estimate total damage.

From Figure 10, for r = 12.5, factor F = 0.77. Thus from Equation (33) the steady-state stress:

$$\sigma_{ss} = 0.77\ \sigma_{in} \qquad\qquad (B-5)$$

The initial stress is estimated by treating the ligament as a clamped beam under pressure loading. The mid-surface length of the beam = 0.0625". For simplicity and conservatism, the loading is assumed to be over this entire length. Thus

$$\sigma_{in} = \frac{3000\ (.0625)^2}{4(.028)^2} = 3737\ \text{psi}$$

From Equation (B-5) σ_{ss} = 0.77 x 3737 = 2878 psi

The ligament in the present example has a large temperature variation across its thickness. The surface temperature of the ligament on the hot gas side is approximately 1325°F while that on the coolant side is about 675°F. If the creep constants are based on an average temperature of 1000°F in determining t_{ss}, then from Equation (32)

$$t_{ss} = \frac{1}{6.2 \times 10^{-16} \times (2.878)^{12.5}} \times \frac{2.3}{12.5} \times \frac{3.737}{16.35 \times 10^3}$$

$$= 4.46 \times 10^8\ \text{seconds}$$

In this case 0.1 t_{ss} is greater than the cycle time of four minutes and the stress remains compressive at the end of the creep period. Thus, there is no creep rupture damage and the life estimate is based on fatigue. The FORTRAN program listed in Appendix C was used for performing the necessary calculations. The input and output are included in this Appendix. Since thinning cannot continue beyond t_{cr}, the fatigue life is estimated to be 206 cycles.

If on the other hand, a more conservative approach is employed and the creep constants for the surface temperature of 1325°F are used in determining t_{ss} (since creep rupture damage occurs at the surface) then from Equation (33):

$$\sigma_{ss} = .8 \, \sigma_{in} = 2990 \text{ psi}$$

From Equation (32):

$$t_{ss} = \frac{1}{5.225 \times 10^{-7} \times (2.99)^{6.65}} \times \frac{2.3}{6.65} \times \frac{3.737}{16.35 \times 10^{3}}$$

$$= .0984 \text{ hrs.} = 354 \text{ seconds}$$

In this case $0.1 \, t_{ss}$ is less than the cycle time of four minutes. The stress at the surface thus becomes tensile and creep rupture damage must be included in the life evaluation. The necessary calculations were again performed using the FORTRAN program listed in Appendix C. The input and output are included in this Appendix.

The output shows that creep rupture damage is now the dominating failure mode, fatigue being relatively small. The estimated life is only twenty cycles.

This example illustrates the sensitivity of the results to the creep properties. It also helps explain the wide discrepancies in the failure life of thrust chambers observed during tests, which have been attributed to local hot spots. The example here shows that if some ligaments do get hotter than others, creep rupture damage could cause early failure. In other instances if the ligaments remain cooler, the chamber lasts much longer.

CONSTANTS INPUT

Q = 0.22800

DELTA = 0.37500E-03 INCHES

E1AVG = 1.4250   PERCENT

H = 0.14000E-01 INCHES

L = 0.40000E-01 INCHES

W = 0.45000E-01 INCHES

P = 0.0000   LBS/INCH

T/CYC = 0.0000   MINUTES

SF = 0.0000

FATIGUE CURVE

CYCLES	STRAIN RANGE
10,000	18,000
100.00	5.9000
4000.0	1.0000
0.50000E+06	0.10000E+00

STRESS-TO-RUPTURE CURVE

HOURS	STRESS (KSI)
0.10000E+00	6.0000
0.80000	4.0000
8.0000	2.5000
100.00	1.5000
1000.0	1.0000

NCYC	TMIN	TMAX	EEQVT	N/ND	STRESS	T/TD	TOTAL USAGE	NF CYCLES
1	0.27801E-01	0.28093E-01	2.8830	0.22575E-02	0.0000	0.0000	0.22575E-02	442
2	0.27603E-01	0.28187E-01	2.9169	0.23131E-02	0.0000	0.0000	0.45706E-02	432
3	0.27404E-01	0.28280E-01	2.9517	0.23708E-02	0.0000	0.0000	0.69414E-02	421
4	0.27206E-01	0.28374E-01	2.9874	0.24308E-02	0.0000	0.0000	0.93722E-02	411
5	0.27007E-01	0.28467E-01	3.0241	0.24932E-02	0.0000	0.0000	0.11865E-01	401
6	0.26809E-01	0.28561E-01	3.0617	0.25581E-02	0.0000	0.0000	0.14424E-01	391
7	0.26610E-01	0.28654E-01	3.1003	0.26256E-02	0.0000	0.0000	0.17049E-01	381
8	0.26412E-01	0.28747E-01	3.1400	0.26959E-02	0.0000	0.0000	0.19745E-01	371
9	0.26213E-01	0.28841E-01	3.1807	0.27690E-02	0.0000	0.0000	0.22514E-01	362
10	0.26015E-01	0.28934E-01	3.2224	0.28451E-02	0.0000	0.0000	0.25359E-01	352
11	0.25816E-01	0.29028E-01	3.2653	0.29243E-02	0.0000	0.0000	0.28283E-01	343
12	0.25618E-01	0.29121E-01	3.3093	0.30067E-02	0.0000	0.0000	0.31290E-01	334
13	0.25419E-01	0.29215E-01	3.3544	0.30926E-02	0.0000	0.0000	0.54385E-01	325
14	0.25221E-01	0.29308E-01	3.4007	0.31820E-02	0.0000	0.0000	0.37565E-01	316
15	0.25022E-01	0.29401E-01	3.4482	0.32751E-02	0.0000	0.0000	0.40840E-01	307
16	0.24824E-01	0.29495E-01	3.4970	0.33721E-02	0.0000	0.0000	0.44212E-01	299
17	0.24625E-01	0.29588E-01	3.5470	0.34731E-02	0.0000	0.0000	0.47685E-01	291
18	0.24426E-01	0.29682E-01	3.5984	0.35784E-02	0.0000	0.0000	0.51263E-01	283
19	0.24228E-01	0.29775E-01	3.6511	0.36882E-02	0.0000	0.0000	0.54952E-01	275
20	0.24029E-01	0.29869E-01	3.7051	0.38026E-02	0.0000	0.0000	0.58754E-01	267
21	0.23831E-01	0.29962E-01	3.7606	0.39219E-02	0.0000	0.0000	0.62676E-01	259
22	0.23632E-01	0.30055E-01	3.8175	0.40462E-02	0.0000	0.0000	0.66722E-01	252
23	0.23434E-01	0.30149E-01	3.8759	0.41759E-02	0.0000	0.0000	0.70898E-01	245
24	0.23235E-01	0.30242E-01	3.9358	0.43112E-02	0.0000	0.0000	0.75209E-01	238
25	0.23037E-01	0.30336E-01	3.9973	0.44523E-02	0.0000	0.0000	0.79662E-01	231
26	0.22838E-01	0.30429E-01	4.0604	0.45996E-02	0.0000	0.0000	0.84261E-01	225
27	0.22640E-01	0.30522E-01	4.1251	0.47533E-02	0.0000	0.0000	0.89015E-01	218
28	0.22441E-01	0.30616E-01	4.1915	0.49137E-02	0.0000	0.0000	0.93928E-01	212
29	0.22243E-01	0.30709E-01	4.2596	0.50812E-02	0.0000	0.0000	0.99009E-01	206
30	0.22044E-01	0.30803E-01	4.3296	0.52560E-02	0.0000	0.0000	0.10427	200
31	0.21846E-01	0.30896E-01	4.4013	0.54387E-02	0.0000	0.0000	0.10970	194
32	0.21647E-01	0.30990E-01	4.4749	0.56295E-02	0.0000	0.0000	0.11533	189
33	0.21449E-01	0.31083E-01	4.5505	0.58288E-02	0.0000	0.0000	0.12116	183
34	0.21250E-01	0.31176E-01	4.6280	0.60371E-02	0.0000	0.0000	0.12720	178
35	0.21051E-01	0.31270E-01	4.7076	0.62548E-02	0.0000	0.0000	0.13345	173
36	0.20853E-01	0.31363E-01	4.7892	0.64824E-02	0.0000	0.0000	0.13994	168
37	0.20654E-01	0.31457E-01	4.8731	0.67204E-02	0.0000	0.0000	0.13994	168
38	0.20456E-01	0.31550E-01	4.9591	0.69693E-02	0.0000	0.0000	0.14666	163
39	0.20257E-01	0.31644E-01	5.0474	0.72297E-02	0.0000	0.0000	0.15363	159
40	0.20059E-01	0.31737E-01	5.1380	0.75021E-02	0.0000	0.0000	0.16086	155
41	0.19860E-01	0.31830E-01	5.2311	0.77872E-02	0.0000	0.0000	0.16836	150
42	0.19662E-01	0.31924E-01	5.3266	0.80857E-02	0.0000	0.0000	0.17615	146
43	0.19463E-01	0.32017E-01	5.4247	0.83982E-02	0.0000	0.0000	0.18423	142
44	0.19265E-01	0.32111E-01	5.5254	0.87255E-02	0.0000	0.0000	0.19263	139
45	0.19066E-01	0.32204E-01	5.6288	0.90683E-02	0.0000	0.0000	0.20135	135
46	0.18868E-01	0.32298E-01	5.7350	0.94275E-02	0.0000	0.0000	0.21042	132
47	0.18669E-01	0.32391E-01	5.8441	0.98041E-02	0.0000	0.0000	0.21985	128
48	0.18471E-01	0.32484E-01	5.9561	0.10197E-01	0.0000	0.0000	0.22965	125
49	0.18272E-01	0.32578E-01	6.0712	0.10608E-01	0.0000	0.0000	0.23985	122
50	0.18074E-01	0.32671E-01	6.1895	0.11039E-01	0.0000	0.0000	0.25046	119
							0.26150	116

51	0.17875E-01	0.32765E-01	6.3110	0.11492E-01	0.0000	0.0000	0.27299	114
52	0.17676E-01	0.32858E-01	6.4359	0.11966E-01	0.0000	0.0000	0.28496	111
53	0.17478E-01	0.32952E-01	6.5643	0.12464E-01	0.0000	0.0000	0.29742	109
54	0.17279E-01	0.33045E-01	6.6962	0.12986E-01	0.0000	0.0000	0.31041	107
55	0.17081E-01	0.33138E-01	6.8319	0.13535E-01	0.0000	0.0000	0.32394	104
56	0.16882E-01	0.33232E-01	6.9714	0.14112E-01	0.0000	0.0000	0.33806	102
57	0.16684E-01	0.33325E-01	7.1148	0.14718E-01	0.0000	0.0000	0.35277	100
58	0.16485E-01	0.33419E-01	7.2624	0.15355E-01	0.0000	0.0000	0.36813	99
59	0.16287E-01	0.33512E-01	7.4142	0.16025E-01	0.0000	0.0000	0.38415	97
60	0.16088E-01	0.33606E-01	7.5703	0.16730E-01	0.0000	0.0000	0.40088	95
61	0.15890E-01	0.33699E-01	7.7311	0.17471E-01	0.0000	0.0000	0.41835	94
62	0.15691E-01	0.33792E-01	7.8966	0.18252E-01	0.0000	0.0000	0.43661	92
63	0.15493E-01	0.33886E-01	8.0670	0.19075E-01	0.0000	0.0000	0.45568	91
64	0.15294E-01	0.33979E-01	8.2424	0.19941E-01	0.0000	0.0000	0.47562	90
65	0.15096E-01	0.34073E-01	8.4232	0.20854E-01	0.0000	0.0000	0.49648	89
66	0.14897E-01	0.34166E-01	8.6094	0.21817E-01	0.0000	0.0000	0.51829	88
67	0.14699E-01	0.34260E-01	8.8013	0.22833E-01	0.0000	0.0000	0.54113	87
68	0.14500E-01	0.34353E-01	8.9991	0.23905E-01	0.0000	0.0000	0.56503	86
69	0.14301E-01	0.34446E-01	9.2031	0.25037E-01	0.0000	0.0000	0.59007	85
70	0.14103E-01	0.34540E-01	9.4135	0.26233E-01	0.0000	0.0000	0.61630	84
71	0.13904E-01	0.34633E-01	9.6306	0.27497E-01	0.0000	0.0000	0.64380	83
72	0.13706E-01	0.34727E-01	9.8546	0.28834E-01	0.0000	0.0000	0.67263	83
73	0.13507E-01	0.34820E-01	10.086	0.30249E-01	0.0000	0.0000	0.70288	82
74	0.13309E-01	0.34913E-01	10.325	0.31746E-01	0.0000	0.0000	0.73463	82
75	0.13110E-01	0.35007E-01	10.572	0.33332E-01	0.0000	0.0000	0.76796	81
76	0.12912E-01	0.35100E-01	10.827	0.35014E-01	0.0000	0.0000	0.80297	81
77	0.12713E-01	0.35194E-01	11.090	0.36797E-01	0.0000	0.0000	0.83977	81
78	0.12515E-01	0.35287E-01	11.363	0.38689E-01	0.0000	0.0000	0.87846	81
79	0.12316E-01	0.35381E-01	11.645	0.40699E-01	0.0000	0.0000	0.91916	80
80	0.12118E-01	0.35474E-01	11.937	0.42834E-01	0.0000	0.0000	0.96199	80
81	0.11919E-01	0.35567E-01	12.240	0.45105E-01	0.0000	0.0000	1.0071	80

CONSTANTS INPUT

Q = 0.22800

DELTA = 0.37500E-03 INCHES

E1AVG = 1.4250   PERCENT

H = 0.14000E-01 INCHES

L = 0.40000E-01 INCHES

W = 0.45000E-01 INCHES

P = 3000.0   LBS/INCH

T/CYC = 4.0000   MINUTES

SF = 0.80000

FATIGUE CURVE

CYCLES	STRAIN RANGE
10.000	18.000
100.00	5.9000
4000.0	1.0000
0.50000E+06	0.10000E+00

STRESS-TO-RUPTURE CURVE

HOURS	STRESS (KSI)
0.10000E+00	6.0000
0.80000	4.0000
8.0000	2.5000
100.00	1.5000
1000.0	1.0000

RESULTS FOR EACH CYCLE

NCYC	TMIN	TMAX	EEQVT	N/ND	STRESS	T/TD	TOTAL USAGE	NF CYCLES
1	0.27801E-01	0.28093E-01	2.8830	0.22575E-02	3.0323	0.21455E-01	0.23713E-01	42
2	0.27603E-01	0.28187E-01	2.9169	0.23131E-02	3.0761	0.23016E-01	0.49042E-01	39
3	0.27404E-01	0.28280E-01	2.9517	0.23708E-02	3.1208	0.24703E-01	0.76116E-01	37
4	0.27206E-01	0.28374E-01	2.9874	0.24308E-02	3.1665	0.26527E-01	0.10507	34
5	0.27007E-01	0.28467E-01	3.0241	0.24932E-02	3.2133	0.28501E-01	0.13607	32
6	0.26809E-01	0.28561E-01	3.0617	0.25581E-02	3.2610	0.30637E-01	0.16926	31
7	0.26610E-01	0.28654E-01	3.1003	0.26256E-02	3.3099	0.32952E-01	0.20484	29
8	0.26412E-01	0.28747E-01	3.1400	0.26959E-02	3.3598	0.35461E-01	0.24300	27
9	0.26213E-01	0.28841E-01	3.1807	0.27690E-02	3.4109	0.38181E-01	0.28395	26
10	0.26015E-01	0.28934E-01	3.2224	0.28451E-02	3.4632	0.41134E-01	0.32793	25
11	0.25816E-01	0.29028E-01	3.2653	0.29243E-02	3.5166	0.44341E-01	0.37519	24
12	0.25618E-01	0.29121E-01	3.3093	0.30067E-02	3.5714	0.47825E-01	0.42602	23
13	0.25419E-01	0.29215E-01	3.3544	0.30926E-02	3.6274	0.51613E-01	0.48073	22
14	0.25221E-01	0.29308E-01	3.4007	0.31820E-02	3.6847	0.55734E-01	0.53964	21
15	0.25022E-01	0.29401E-01	3.4482	0.32751E-02	3.7434	0.60221E-01	0.60314	21
16	0.24824E-01	0.29495E-01	3.4970	0.33721E-02	3.8035	0.65110E-01	0.67162	20
17	0.24625E-01	0.29588E-01	3.5470	0.34731E-02	3.8651	0.70440E-01	0.74553	20
18	0.24426E-01	0.29682E-01	3.5984	0.35784E-02	3.9282	0.76254E-01	0.82537	20
19	0.24228E-01	0.29775E-01	3.6511	0.36882E-02	3.9928	0.82602E-01	0.91166	20
20	0.24029E-01	0.29869E-01	3.7051	0.38026E-02	4.0591	0.89838E-01	1.0053	19

APPENDIX C

FORTRAN PROGRAM FOR

FATIGUE AND CREEP RUPTURE DAMAGE EVALUATION

```
      PROGRAM CYCLES
      REAL NF,L,NO
      DIMENSION CYCLE(20),STRAIN(20),SIG(20),TIME(20)
C
C
C         G= EXPONENT IN STRESS-STRAIN LAW.
C     DELTA= DEFORMATION PER CYCLE
C     E1AVG= AVERAGE HOOP STRAIN (PERCENT)
C         H= HALF THE HEIGHT OF LIGAMENT
C         L= LENGTH OF LIGAMENT
C         W= WIDTH OF RIB
C         P= PRESSURE (LBS/IN)
C       TPC= TIME PER CYCLE (MINUTES)
C        SF= SHAPE FACTOR
C
C
C     TO ELIMINATE CREEP EFFECTS, ENTER O FOR P, TPC AND SF
C
      READ(15,*) Q,DELTA,E1AVG,H,L,W,P,TPC,SF
C
C     INPUT FATIGUE CURVE
C     NFAT=NUMBER OF DATA POINTS ON FATIGUE CURVE TO BE INPUT (MAX OF 20)
C     CYCLE=CYCLES FOR EACH DATA PT
C     STRAIN=STRAIN RANGE FOR EACH PT
C
      READ(15,*) NFAT
      READ(15,*) (CYCLE(I),I=1,NFAT)
      READ(15,*) (STRAIN(I),I=1,NFAT)
C
C     INPUT STRESS-TO-RUPTURE CURVE
C     NRUP=NUMBER OF DATA POINTS TO BE INPUT (MAX OF 20)
C     SIG=STRESS FOR EACH DATA PT (KSI)
C     TIME=TIME FOR EACH DATA PT (HOURS)
C
      READ(15,*) NRUP
      READ(15,*) (TIME(I),I=1,NRUP)
      READ(15,*) (SIG(I),I=1,NRUP)
C
C     PRINT SUMMARY OF INPUT
C
      WRITE(16,500) Q,DELTA,E1AVG,H,L,W,P,TPC,SF
      DO 5 I=1,NFAT
    5 WRITE(16,600) CYCLE(I),STRAIN(I)
      WRITE(16,620)
      DO 7 I=1,NRUP
    7 WRITE(16,600) TIME(I),SIG(I)
C
C     CALCULATE CYCLES TO FAILURE
C
      WRITE(16,700)
      USEAGE=0.0
      NCYC=0
      C=(Q-1)/Q
      TPC=TPC/60
   10 NCYC=NCYC+1
      TMIN=(2*H*(L+W)-NCYC*DELTA*W)/(L+W)
      TMAX=(2*H*(L+W)**2+NCYC*DELTA*L*W)/(L+W)**2
      T=TMAX/TMIN
      E1MIN=E1AVG*C*(T-1)/(T**C-1)
      E1=E1MIN
      E2=E1AVG
      EEQVT=SQRT((E1-E2)**2+(2*E1+E2)**2+(2*E2+E1)**2)*SQRT(2.)/3
      DO 20 I=2,NFAT
      IF(EEQVT.LE.STRAIN(I-1) .AND. EEQVT.GE.STRAIN(I)) GOTO 30
```

```fortran
   20 CONTINUE
      WRITE(16,300) EEQVT
      STOP
   30 ND=EXP(ALOG(EEQVT/STRAIN(I-1))/ALOG(STRAIN(I)/STRAIN(I-1))*
     2ALOG(CYCLE(I)/CYCLE(I-1))+ALOG(CYCLE(I-1)))

C
C     CALCULATE TIME TO RUPTURE
C
      TD=1
      IF(P.EQ.0.0) GO TO 60
      PM=SF*P*(L+W/2)**2/24
      S=6*PM/TMIN**2
      S=S/1000
      DO 40 I=2,NRUP
      IF(S.LE.SIG(I-1) .AND. S.GE.SIG(I)) GO TO 50
   40 CONTINUE
      IF(S.LT.SIG(NRUP)) GO TO 45
      TD=EXP(ALOG(TIME(2))-ALOG(SIG(2)/S)/ALOG(SIG(2)/SIG(1))*
     2 ALOG(TIME(2)/TIME(1)))
      GO TO 60
   45 TD=EXP(ALOG(TIME(NRUP-1))-ALOG(SIG(NRUP-1)/S)/
     2 ALOG(SIG(NRUP-1)/SIG(NRUP))*ALOG(TIME(NRUP-1)/TIME(NRUP)))
      GO TO 60
   50 TD=EXP(ALOG(S/SIG(I-1))/ALOG(SIG(I)/SIG(I-1))*
     2 ALOG(TIME(I)/TIME(I-1))+ALOG(TIME(I-1)))

C
C     COMPUTE CUMULATIVE DAMAGE
C
   60 USEAGE=USEAGE + 1./ND + TPC/TD
      NF=(1-USEAGE)/(1./ND + TPC/TD) + NCYC
      WRITE(16,800) NCYC,TMIN,TMAX,EEQVT,1./ND,S,TPC/TD,USEAGE,IFIX(NF)
      IF(USEAGE.LT.1.0) GO TO 10
      STOP

C
C     FORMATS
C
  300 FORMAT(1H0,"THE STRAIN RANGE OF ",G12.5,
     1 " IS NOT ON THE FATIGUE CURVE SUPPLIED")
  350 FORMAT(1H0,"THE STRESS OF ",G12.5,
     1 " IS NOT ON THE STRESS-TO-RUPTURE CURVE SUPPLIED")
  500 FORMAT(1H1,12X,"CONSTANTS INPUT"//11X,"    Q= ",G12.5//11X,
     2 "DELTA =",G12.5," INCHES"//11X,
     3 "E1AVG =",G12.5," PERCENT"//11X,
     4 "    H =",G12.5," INCHES"//11X,
     5 "    L =",G12.5," INCHES"//11X,
     6 "    W =",G12.5," INCHES"//11X,
     7 "    P =",G12.5," LBS/INCH"//11X,
     8 "T/CYC =",G12.5," MINUTES"//11X,
     8 "   SF =",G12.5////18X,
     9 "FATIGUE CURVE"//14X,"CYCLES",7X,"STRAIN RANGE"/)
  600 FORMAT(1H ,6X,2(4X,G12.5))
  620 FORMAT(1H0///13X,"STRESS-TO-RUPTURE CURVE"//13X,
     2 " HOURS",8X,"STRESS (KSI)"/)
  700 FORMAT(1H1,46X,"RESULTS FOR EACH CYCLE"//
     2 5X,"NCYC",6X,"TMIN",11X,"TMAX",11X,"EEQVT",10X,"N/ND",
     3 10X,"STRESS",10X,"T/TD",9X,"TOTAL USAGE",3X,"NF CYCLES"/)
  800 FORMAT(1H ,I7,7(3X,G12.5),I8)
      END
```

APPENDIX D

SYMBOLS

A	-	area
$\overline{A}$	-	equation arbitrary positive scalar
B	-	material constant in Norton's creep law
D	-	constant in Ramberg-Osgood stress strain law
e	-	elastic strain
E	-	modulus of elasticity
$\underline{F}(r)$	-	Factor in Figure 10
$\overline{F}(r)$	-	Factors in Table I
$2H$	-	thickness of ligament
k	-	$\sqrt{1 - s^2}$; also thermal conductivity
K	-	curvature
ℓ	-	width of ligament in hoop direction
m	-	generalized bending stress variable
M	-	bending moment in ligament
M_o	-	yield bending moment
n	-	generalized hoop stress variable
N	-	hoop force in ligament; also number of cycles
N_o	-	yield hoop force
p	-	pressure
q	-	exponent in Ramberg-Osgood stress strain law
r	-	exponent in Norton's creep law
s	-	generalized shear stress variable
S	-	shear force in ligament
S_y	-	average yield stress in tension
$S_{y_{min}}$	-	ligament yield strength for minimum $\alpha(T_i - T_o)$
$S_{y_{max}}$	-	ligament yield strength for maximum $\alpha(T_i - T_o)$

82

t	-	time
t_{cr}	-	critical ligament thickness
t_N	-	thinning after N cycles
t_{min}	-	minimum ligament thickness
t_{max}	-	maximum ligament thickness
t_{ss}	-	time to reach steady state distribution
T	-	temperature
T_i	-	average temperature of ligament
T_o	-	average temperature of closeout wall
w	-	width of rib

α	-	coefficient of thermal expansion; also stress ratio σ_2/σ_1
γ	-	shear strain
δ	-	deflection per cycle
δ_1	-	deflection due to moment
δ_2	-	deflection due to shear
δ_3	-	creep induced deflection
Δ_p	-	pressure difference between coolant pressure and combustion gas pressure
$\Delta\varepsilon'_{p_1}$	-	inelastic strain range in hoop direction due to differential thermal expansion
$\Delta\varepsilon''_{p_1}$	-	correction to plastic strain range in hoop direction due to thermally induced bending
ε_1	-	strain
ε_1	-	hoop strain
ε_{1avg}	-	average hoop strain in ligament
ε_{1min}	-	hoop strain in minimum ligament section
$\overline{\varepsilon}_{2min}$	-	axial strain in minimum ligament section
$\overline{\varepsilon}_{cr}$	-	critical effective strain

SYMBOLS - continued

$\bar{\varepsilon}_{min}$	-	effective in minimum ligament section
θ	-	generalized bending strain variable
λ	-	generalized hoop strain variable
ν	-	Poisson's ratio
σ	-	stress
σ_1	-	hoop stress
σ_2	-	axial stress
$\Delta\sigma_c$	-	creep relaxation stress
σ_{in}	-	initial pressure induced bending stress
σ_p	-	peak stress
σ_{ss}	-	steady state stress
T	-	dimensionless time
ϕ	-	generalized shear strain variable
$\cdot$	-	dot above symbol denotes rate

84

NAS3-23343

O'Donnell & Associates

"Development of a Simplified Procedure for Rocket Engine Thrust Chamber
Life Prediction with Creep"

DISTRIBUTION LIST FOR FINAL REPORT - CR 168261

<u>Name</u>   <u>No. of Copies</u>

National Aeronautics & Space Administration
Lewis Research Center
21000 Brookpark Road
Cleveland, Oh 44135

Attn: Contracting Officer, MS 500-305	1
Technical Utilization Office, MS 7-3	1
Technical Report Control Office, MS 5-5	1
AFSC Liaison Office, MS 501-3	2
Library, MS 60-3	2
Office of Reliability & Quality Assurance, MS 500-211	1
N. T. Musial, MS 500-318	1
H. J. Kasper, Project Manager, MS 500-107	10
D. R. Ryan, MS 501-5	1
H. G. Price, MS 501-6	3
C. A. Aukerman, MS 501-6	1
G. M. Reck, MS 501-6	1
R. J. Quentmeyer, MS 501-6	1
G. R. Halford, MS 49-6	2

National Aeronautics & Space Administration
Headquarters
Washington, D.C. 20546

Attn: RST-5/E. A. Gabris	1
RST-5/F. W. Stephenson	1
RSS-5/R. F. Carlisle	1

National Aeronautics & Space Administration
Ames Research Center
Moffett Field, CA 94035

Attn: Library   1

National Aeronautics & Space Administration
Flight Research Center
P. O. Box 273
Edwards, CA 93523

Attn: Library   1

National Aeronautics & Space Administration
Goddard Space Flight Center
Greenbelt, MD 20771

Attn: Library   1

National Aeronautics & Space Administration
George C. Marshall Space Flight Center
Marshall Space Flight Center, AL 35812

Attn: Library   1
      J. L. Sanders/PD13   1
      R. Richmond/EP24   1
      J. A. Lombardo/EP21   1
      C. R. Bailey/EP23   1
      D. E. Pryor/EP23   1
      S. F. Morea/EP01   1

National Aeronautics & Space Administration
John F. Kennedy Space Center
Kennedy Space Center, FL 32899

Attn: Library   1

National Aeronautics & Space Administration
Lyndon B. Johnson Space Center
Houston, TX 77058

Attn: Library   1

National Aeronautics & Space Administration
Langley Research Center
Hampton, VA 23665

Attn: Library   1

NASA Scientific & Technical Information Facility
P. O. Box 8757
Baltimore-Washington Intnl. Airport
Baltimore, MD 21240

Attn: Accessioning Department   10

Office of the Director of Defense
Research & Engineering
Washington, D.C. 20301

Attn: Office of Assistant Director (Chemical Technology)   1

Jet Propulsion Laboratory
4800 Oak Grove Drive
Pasadena, CA 91103

Attn: Library   1

Defense Documentation Center
Cameron Station, Bldg. 5
5010 Duke St.
Alexandria, VA 22314

Attn: TISIA   1

Advanced Research Projects Agency
Washington, D.C. 20525

Attn: Library   1
86

Aerojet Tech Systems Co.
P. O. Box 13222
Sacramento, CA 95813

Attn: Library   1
     D. C. Rousar   1
     R. W. Michel   1

Aeronautical Systems Division
Air Force Systems Command
Wright-Patterson Air Force Base
Dayton, OH 45433

Attn: Library   1
     E. E. Bailey   1

Air Force Rocket Propulsion Laboratory (RPM)
Edwards, CA 93523

Attn: Library   1
     R. R. Weiss   1

Air Force Office of Scientific Research
1400 Wilson Blvd.
Arlington, VA 22209

Attn: Library   1

U.S. Air Force, Office of Information
Office of Sec. of Air Force
The Pentagon
Washington, D.C. 20333

Attn: Library   1

Air Force Aero Propulsion Laboratory
Research & Technology Division
U. S. Air Force Systems Command
Wright Patterson AFB, OH 45433

Attn: Library (APRP)   1

Arnold Engineering Development Center
Air Force Systems Command
Tullahoma, TN 37388

Attn: Library   1

Bureau of Naval Weapons
Department of the Navy
Washington, D.C.

Attn: Library   1

U. S. Naval Research Laboratory
Washington, D.C. 20390

Attn: Library   1

U. S. Army Research Office (Durham)
Box CM, Duke Station
Durham, NC 27706

Attn: Library   1

U. S. Army Missile Command
Redstone Scientific Information Center
Redstone Arsenal, AL 35808

Attn: Document Section   1

U. S. Naval Missile Center
Point Mugu, CA 93041

Attn: Technical Library   1

U. S. Naval Weapons Center
China Lake, CA 93557

Attn: Library   1

Battelle Memorial Institute
505 King Avenue
Columbus, OH 43201

Attn: Library   1

Bell Aerosystems Inc.
Box 1
Buffalo, NY 14240

Attn: Library   1

Boeing Company, Space Division
P. O. Box 868
Seattle, WA 98124

Attn: Library   1

Chemical Propulsion Information Agency
Applied Physics Laboratory
8621 Georgia Avenue
Silver Spring, MD 20910   1

General Dynamics/Convair
P. O. Box 1128
San Diego, CA 92112

Attn: Library   1

General Electric Company
Missiles & Space Systems Center
Valley Forge Space Tech. Center
P. O. Box 8555
Philadelphia, PA 19101

Attn: Library   1
88

Grumman Aerospace Corp.
Bethpage, L. I., NY   11714

Attn: Library   1

Lockheed Missiles & Space Co.
P. O. Box 504
Sunnyvale, CA   94088

Attn: Library   1

Marquardt Corporation
16555 Staticoy Street
Box 2013 South Annex
Van Nuys, CA   91409

Attn: Library   1

Martin-Marietta Corp.
P. O. Box 179
Denver, CO   80201

Attn: Library   1

McDonnell Douglas Astronautics
5301 Bolsa Avenue
Huntington Beach, CA   92547

Attn: Library   1

Philco-Ford Corporation
Aeronautics Div.
Ford Rd.
Newport Beach, CA   92663

Attn: Library   1

Purdue University
Lafayette, IN 47907

Attn: Library   1

Rocketdyne
A. Div. of Rockwell Corp.
6633 Canoga Avenue
Canoga Park, CA   91304

Attn: Library   1
      G. Bremer   1
      F. M. Kirby   1

Rocket Research Corporation
Willow Road at 116th Street
Redmond, WA   98052

Attn: Library   1

Thiokol Chemical Corporation
P. O. Box 1000
Newton, PA 18940

Attn: Library   1

TRW Systems, Inc.
1 Space Park
Redondo Beach, CA 90278

Attn: Library   1

United Aircraft Corporation
Pratt & Whitney Division
Florida Research & Development Center
P. O. Box 2691
West Palm Beach, FL 33402

Attn: Library   1

United Technologies Research Center
East Hartford, CT

Attn: Library   1

Lockheed Missiles & Space Co., Inc.
P. O. Box 1103
Huntsville, AL 35807

Attn: W. H. Armstrong   1

90